Proper Generalised Decomposition for heat and moisture multizone modelling

Julien Berger, Sihem Guernouti, Monika Woloszyn, Francisco Chinesta

Proper Generalised Decomposition for heat and moisture multizone modelling

Julien Berger [a,*], Sihem Guernouti [b], Monika Woloszyn [c], Francisco Chinesta [d]

[a] *Thermal Systems Laboratory, Department of Mechanical Engineering, Pontifical Catholic University of Parana, Nantes, France*
[b] *Cerema, Dter Ouest, Nantes, France*
[c] *LOCIE, UMR CNRS 5271, Université de Savoie, Chambéry, France*
[d] *GEM, UMR CNRS, Ecole Centrale de Nantes, France*

Innovative and efficient ways to perform numerical simulations are worth investigations to reduce the computational complexity of building models and permit to solve complex problems. This paper proposes a Proper Generalised Decomposition (PGD) model reduction technique for heat and moisture multizone modelling. First, the transient multizone problem is written using PGD formalism and solved in a non-incremental way to assess hygrothermal fields. The computational complexity and accuracy of results of the reduced-order model and the large original model are compared, highlighting that the fields are precisely represented with the PGD resolution. The complexity of the reduced-order model is lower, offering interesting numerical savings, particularly when the number of the building zones increases.

The second advantage of the method is for solving parametric problems. Two illustrations are proposed. The first considers a climate and ventilation flow rates parametric multizone problem. The PGD model analyse the behaviour of building zones as a function of these two extra-parameters. For the second, an initial condition and source-term PGD parametric solution is computed. It is then coupled with a wall model to perform whole-building hygrothermal simulation. For both studies, the model represents accurately the hygrothermal fields in the different zones with important computational savings.

1. Introduction

Annex 41 of the International Energy Agency reported on most detailed models and their successful applications for accurate assessment of hygrothermal transfer in buildings [1]. To accurately assess the hygrothermal behaviour of buildings, one possibility is to couple two different models:

1 a *wall model*, simulating heat and mass transfer in multilayer walls. Several one- (1D) [2–4], two- or three- (2 or 3D) dimensional [5–10] models can be found in the literature for commercial or research uses.
2 a *multizone model*, calculating the heat and mass balance of moist air volumes of a number of zones composing a building. The balance is calculated as a function of the heat and vapour sources or sinks of each zone. Examples of the multizone model are given in [11,12].

The coupling of these two models makes it possible to perform *whole-building hygrothermal simulation*. This type of model is called a *global* model. Examples of the association of a 1-D wall model with a multizone model are found in various successful applications [13–17,12,18,19]. The association of a 2- or 3-D wall model with a multizone model is a complex task due to the substantial numerical complexity of such models [20–24]. The numerical complexity comes from the number of equations resulting from the discretisation together with non-linear couplings. Indeed, the space domain of the wall model is considerable. One wall assembly with a mesh of approximately 1 cm^3 results in about 10^6 nodes for a 3D simulation. Similarly, the time domain is also large as simulations are expected to cover at least 1 year with fine discretisation (minutes). Problems become even more complex when a parametric solution is searched for, such as evaluating the behaviour of a building as a function of the outdoor climate. Couplings between heat and mass transfers equations add also numerical complexity.

To reduce the computational complexity of the *global* model, an innovative and efficient numerical simulation methods are worth investigation. Model order reduction techniques, aiming at decreasing the number of equations to be solved, are advantageous alternatives. For building physics issue investigated herein, these

* Corresponding author.
E-mail address: julien.berger@pucpr.edu.br (J. Berger).

Nomenclature

Latin letters

A	surface (m^2)
g	moisture flow (kg/s)
L_v	latent heat evaporation (J/kg)
P	vapour pressure (Pa)
R_v	gas constant for water (J/(kg K))
t	time (s)
V	volume (m^3)
z	zone number
C	heat capacity (J/(kg K))
K_l	liquid permeability (s)
m	mass (kg)
q	heat flow (W)
RH	relative humidity (–)
T	temperature (K)
w	vapour content (% kg)

Greek letters

α	convective heat transfer coefficient (W/(m^2K))
β	convective mass transfer coefficient (s/m)
ρ	density (kg/m^3)
δ_v	vapour permeability (s)
λ	thermal conductivity (W/(m K))
ξ	moisture capacity (kg/(m^3 Pa))

subscript

a	air
m	material
v	vapour
z	zone
l	liquid
s	source
w	walls

techniques can be applied to model transfer processes in materials and/or to multizone moist air model. In [25], a reduced order model based on Proper Generalised Decomposition (PGD) was proposed to solve 2D coupled heat and moisture transfer in materials. As a result, PGD showed its efficiency in solving such problems with a low computational cost. It was demonstrated that time evolution and amplitude of hygrothermal fields in materials are accurately represented with PGD solution. Therefore, next step to be done is applying model order reduction techniques on a multizone model.

In literature, to our knowledge, a few studies can be found on the reduction of complexity of the building multizone model. Some analytical solutions based on state-space method have been proposed to solve the thermal multizone model [26,27] or the pollutant transfers multizone model [28,29]. In [30], the thermal multizone model is solved using truncation model reduction technique.

This paper proposes to explore the application of PGD, an innovative model reduction technique, to multizone simulation. The features of the PGD method will be exposed and illustrated on a case study. The latter remains simple as the main purpose of the present work is to show the relevance of the model order reduction techniques for multizone simulation. In the first part, the transient hygrothermal multizone problem is written using the PGD formalism and solved in a non-incremental way to assess indoor temperatures and vapour pressures. The computational complexity and the accuracy of the results of the reduced order model (ROM) is compared with the classic approaches to solve the problem (using finite differences). This classic approach is called the large original model (LOM) in the manuscript.

The second part of the paper investigates the features of the PGD that enables to introduce model parameters as extra coordinates for solving complex parametric problems. The first case study will consider a multizone problem with climate and ventilation rate as parameters of the problem. The second one considers a multizone problem with initial conditions as well as heat and moisture sources as parameters. The results are compared with the commercial validated model *WUFI plus*, and numerical features of the PGD method applied to whole building heat and moisture multizone simulation are discussed.

2. The multizone model and the Proper Generalised Decomposition method

2.1. Hygrothermal multizone equations

For moist air multizone modelling, a whole building is broken down into N_z perfectly mixed air zones. Each zone is represented by one node defined as a moist air volume governed by heat and mass conservation equations detailed in Appendix A. Each volume receives a mass or heat source or sink term. Fields of interest are temperature T and vapour pressure P of each control volume. Their time evolutions are the solution to the following problem:

Problem 1. $\forall z = \{1, \ldots, N_z\}$, Find $T_z(t) : \Omega_t \longrightarrow \mathbb{R}$ and $P_z(t) : \Omega_t \longrightarrow \mathbb{R}$

$$\begin{bmatrix} s_{11} & s_{12} \\ s_{21} & s_{22} \end{bmatrix}_z \begin{bmatrix} \frac{dT}{dt} \\ \frac{dP}{dt} \end{bmatrix}_z = \begin{bmatrix} q \\ g \end{bmatrix}_z \quad in\ \Omega_t \tag{i}$$

$$\begin{bmatrix} T & P \end{bmatrix}_z = \begin{bmatrix} T_0 & P_0 \end{bmatrix}_z \quad t = t_0 \tag{ii}$$

With s_{ij} coefficients of the storage matrix. q and g are the source terms depending on fields T and P and thus time and zones. The physical description of these terms is given in Appendix A. Problem 1 is called the multizone problem. It is a CAUCHY problem and requires an initial condition to be solved. The multizone algorithm is based on a domain decomposition techniques that subdivide the whole building into a finite number of zones. It is therefore composed of a system of $2 \times N_z$ ordinary differential equations to be solved over time domain Ω_t. Each equation corresponds to the local balance of each zone. Thus, Problem 1 is called the *local* problem. It will be considered for the present study and PGD model order reduction technique will be applied on Problem 1. In addition, resolution using explicit time integration of Problem 1 over time domain $Omega_t$, discretised into N_t elements will also be performed. This classical approach will be refereed as "large original model" (LOM) in the following manuscript.

2.2. Proper Generalised Decomposition

The PGD method originates in the radial space-time separated representation proposed by Ladeveze in 1985 [31]. In 2006, the separated representations were extended to the multidimensional case by Chinesta and co-workers [32]. Interested readers can see Chinesta et al. [33,34] for additional details on the method as well as [35] for an introduction. This strategy has been successfully applied and validated for various industrial applications. For instance, the PGD resolution was applied to quantum mechanics (Schroedinger equation) [36], kinetics theory (Fokker–Planck equation non-Newtonian fluids) [37,38], phase separation in heterogeneous mixtures (Langer equation) [39], virtual surgery (forces, vibrations, etc.) [40–42], non-linear stochastic problems (Burgers equation, 2D non-linear diffusion problems) [43], multi-scale and multiphysics problems (visco plasticity, damage, etc.) [44], computational fluid

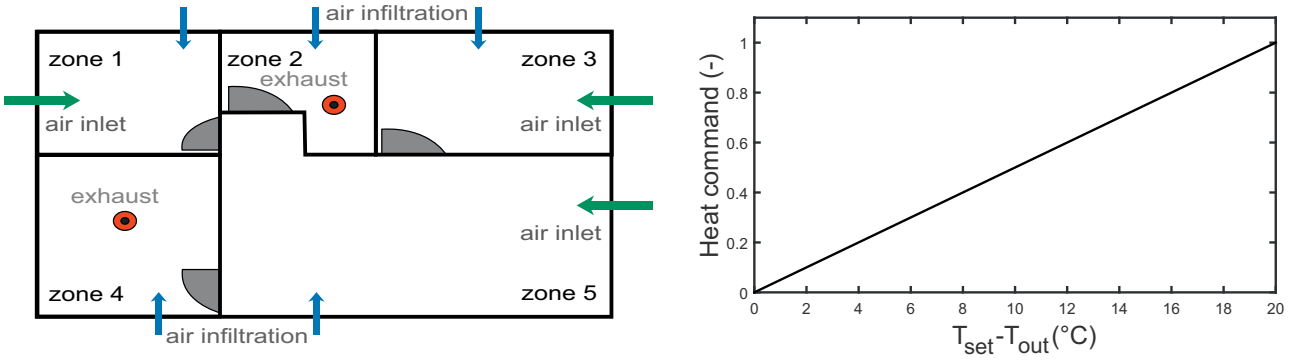

(a) Case study (b) Heat command

Fig. 1. Schematic view of the case study (a) and heating power control of each zone's heating system (b).

dynamics (anisotherm Navier–stokes problems) [45,46], heat and moisture transfers in building materials [25], etc.

The PGD is an *a priori* method, i.e. there is no previous resolution of the large original model to build the reduced order model. The PGD resolution method makes it possible to solve transient problems in a non-incremental way. It is based on the hypothesis that the solution Θ of a problem depending on the independent coordinates $(x_i)_{1\leq i\leq d} \in \Omega^d$ is approximated using a finite sum representation:

$$\Theta(x_1, x_2, \ldots, x_d) \approx \sum_{i=1}^{M} F_1^i(x_1) \cdot F_2^i(x_2) \cdots F_d^i(x_d) \tag{2}$$

The approximation functions $(F_i^n)_{\{1\leq i\leq d\},\{1\leq n\leq M\}}$ are computed using an iterative procedure. The values for $i=1$ are determined using initial conditions. Then, successive iterations, called *enrichment steps*, using an alternating direction fixed-point strategy enable calculating terms of the sum for $i>1$. The procedure is stopped when convergence is reached, i.e. when Eq. (2) inserted into Problem 1 results in a residual smaller than a fixed tolerance. M is called the number of modes. The interested reader can refer to [35] for further details and [25] for building physics applications.

3. Model reduction technique for the building multizone model

First, Problem 1 will be solved using the PGD model reduction technique. For this purpose, Problem 1 is modified by introducing the integer coordinate z, representing each zone. The new problem is written as:

Problem 2. Find $T(z,\ t): \Omega = \Omega_z \times \Omega_t \longrightarrow \mathbb{R}$ and $P(z,\ t): \Omega = \Omega_z \times \Omega_t \longrightarrow \mathbb{R}$

$$\begin{bmatrix} s_{11} & s_{12} \\ s_{21} & s_{22} \end{bmatrix} \begin{bmatrix} \dfrac{\mathrm{d}T}{\mathrm{d}t} \\ \dfrac{\mathrm{d}P}{\mathrm{d}t} \end{bmatrix} = \begin{bmatrix} q \\ g \end{bmatrix} \quad \text{in } \Omega \tag{i}$$

$$\begin{bmatrix} T & P \end{bmatrix}^T = \begin{bmatrix} T_0 & P_0 \end{bmatrix}^T \quad \text{Initial condition at } t_0 \tag{ii}$$

Problem 2 is defined for $(z,\ t) \in \Omega = \Omega_z \times \Omega_t$. Indeed, the evolution of fields T and P depends on time t. Since they also differ for each zone, it is assumed that T and P also vary with the spatial coordinate $z \in \{1, \ldots, N_z\}$. This coordinate z does not have a physical meaning. It merely represents the number of the zone considered.

Therefore, the PGD solution to Problem 2 is sought as a separated representation of time t and space z, the first having a continuous nature (and having been discretised), the second being discrete because only integer values referring to the zones are used:

$$T(z,\ t) = \sum_{i=1}^{M} F_1^i(z) F_2^i(t) \tag{3a}$$

$$P(z,\ t) = \sum_{i=1}^{M} G_1^i(z) G_2^i(t) \tag{3b}$$

The solution procedure is fully detailed in [35] and illustrated for Problem 2 in Appendix B.

Table 1
Parameters of the case study.

	Zone 1	Zone 2	Zone 3	Zone 4	Zone 5
Surface area (m^2)	12.25	10.5	15.75	15.75	36.75
Airflow due to airtightness (m^3/h)	9.8	4.2	11.2	11.2	16.8
Airflow due to windows inlet (m^3/h)	22.5	0	22.5	0	45
Mechanical exhaust v (m^3/h)	0	45	0	45	0
Heating power (W)	202.50	172.5	258	258	306
Vapour source (g/h)	0	240	0	240	0

3.1. Case study

A case study was chosen to evaluate the reduction technique for the multizone model. It represents a 91 m^2 family house illustrated in Fig. 1(a). The building is ventilated. Zones 2 and 4 have a mechanical exhaust with a flow rate of $v = 45\ m^3/h$. Zones 1, 3 and 5 have windows containing air inlets. The air tightness coefficient at 4 Pa of the building is 0.4 $m^3/h/m^2$ (airflow per surface of building envelope). Main data for each zone are given in Table 1. It is considered that 25% of the total entering flow rate is extracted in zone 2 and 75% in zone 4.

In addition, the building is heated and each zone has a heating power given in Table 1. The heating is controlled as a function of outside temperature T_{out} and the set-point temperature $T_{set} = 18\ ^\circ C$ as illustrated in Fig. 1(b). For instance, if the difference between the outside and the set-point temperature equals 20 °C, zone 1 receives a heat power of 202.5 W. Moisture is generated from 8 h to 10 h and from 16 h to 19 h at the rate of 240 g/h in zones 2 and 4. The

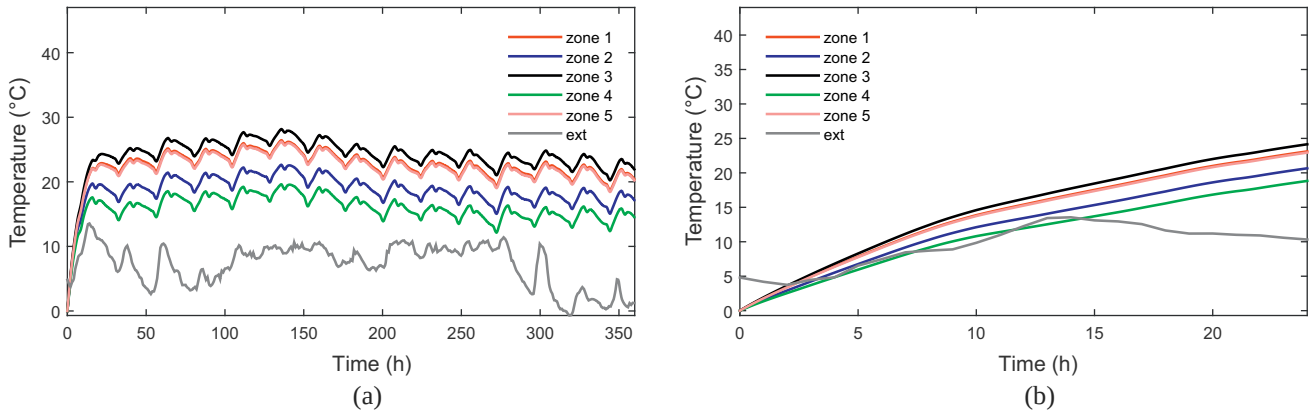

Fig. 2. Temperature in each zone for the 15 days (a) and for the 1st day (b) over time.

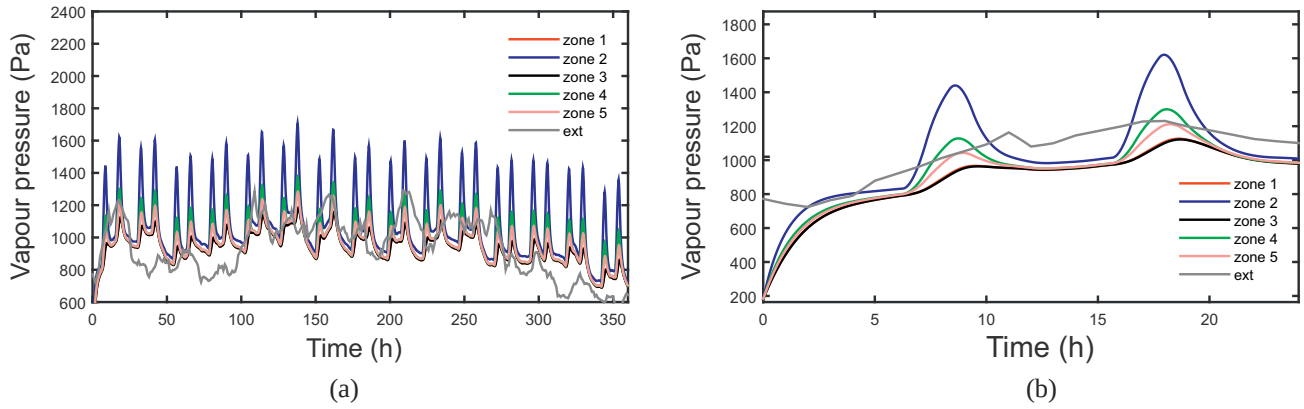

Fig. 3. Vapour pressure in each zone for the 15 days (a) and for the 1st day (b) over time.

outside climate corresponds to the standard climate in France (zone *H1a* [47]). Outside temperature and vapour pressure are given in Figs. 2 and 3(a). The initial conditions for all zones are $T = 0\,^{\circ}\mathrm{C}$ and $RH = 0.3$. The airflows between zones $m_{a,j}$ are considered constant. In addition, heat and moisture transfers through building envelope are note included here.

The problem is solved for a period of 15 days (360 h) with a constant time step of 10 s. The PGD reduced order model (PGD ROM) is compared with the large original model (LOM) associated with Problem 1. The latter is built using a finite difference method. Both models are implemented in MATLAB environment [48].

3.2. Results and discussion

3.2.1. Physical analysis

The main interest is to highlight that the PGD reduced order model correctly translates the physical behaviour of the building. Figs. 2 and 3 give the temperature and vapour pressure for each zone over time. A detail for the first day is proposed to give a more precise analyse. In addition, the inter-zonal heat and vapour flows are illustrated in Fig. 4. Flows are positive when they contribute to increasing the temperature or moisture content in the corresponding zone.

The PGD reduced order model computes temperature and vapour pressure in each zone, as can be noted in Figs. 2 and 3. The temperature in zone 3 is higher than in zone 1 because the former receives more heat from the heating system. The temperature in zone 5 is higher than in zone 4 for the same reason. The heating power is high in zone 5, as can be noted in Table 1. However, the temperature in zone 5 is not as high because of large flows of air moving to zone 2 and 4 to be extracted. In addition, Fig. 4(a) illustrates that all the flows exiting zones 1, 3 and 5 are extracted in zones 2 and 5. As 75% of airflow is extracted in zone 4, the heat flow entering zone 4 is higher than that in zone 2. It can be noticed also that the outside temperature is inferior to inside temperature and contributes to decreasing the energy balance.

In Fig. 3(a) and (b), vapour pressure in zone 2 and zone 4 is greater than in other zones because they receive a daily generation of vapour. Exhaust in zone 4 is higher and therefore this zone has a lower vapour pressure than zone 2. The sum of vapour flows in zones 1, 2 and 3 is equal to the sum of vapour flows extracted in zone 4 and 5.

Fig. 5 compares the results of the large original model and the PGD reduced order model. The large original model corresponds to a classic solution of Problem 1.

It can be noted that there is a very good agreement between the two solutions in Fig. 5. The relative difference is lower than 0.1% for both temperature and vapour pressure. Considering these results, the PGD solution to the problem succeeds in precise representation of temperature and vapour pressure in all zones.

3.2.2. Main features of numerical resolution

To solve Problem 1, two options are possible. First, the usual way is to use the large original model, in which case, Problem 1 is solved for each zone. This means that each local problem needs to be considered. Each differential balance equation for any zone is solved using classical time-integration algorithms. Roughly, using an explicit scheme, the calculations are repeated N_t times (N_t being the number of time-steps). In the second approach, the PGD resolution, a discrete spatial coordinate z is assumed to represent

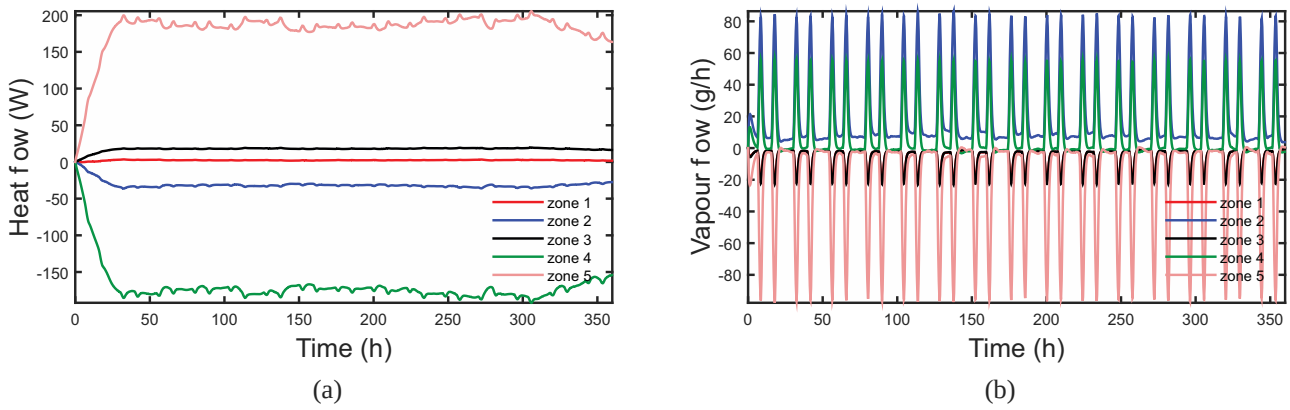

(a) (b)

Fig. 4. Heat and vapour flow moving into each zone over time.

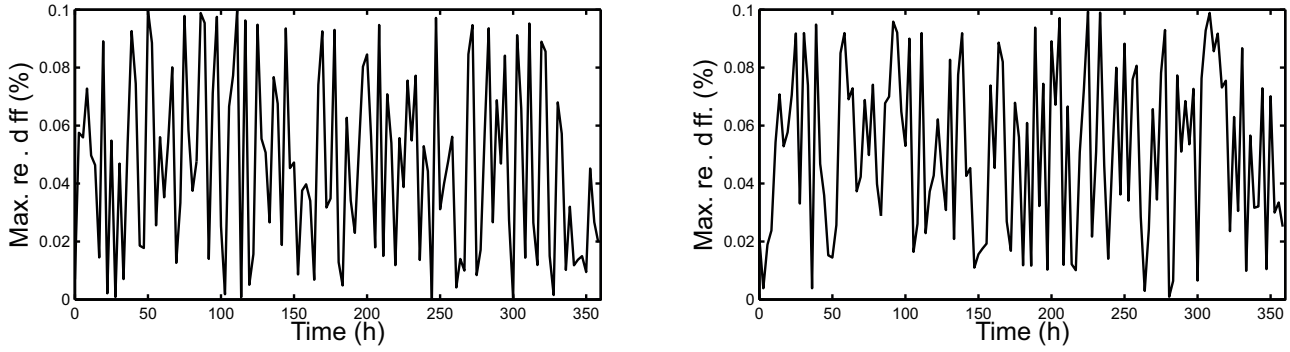

(a) Temperature (b) Vapour pressure

Fig. 5. Difference between PGD reduced order model and large original model.

the considered zone. In this way, all local problems of the N_z zones are gathered into a global Problem 2. This possibility avoids solving the N_z differential equations of Problem 1 to compute the solution in each zone. Problem 2 is solved once to calculate the field of interest in all zones very accurately although the increase of the model dimension.

Nine modes were used to compute the PGD solution. Fig. 6 shows the decrease of the residual of Problem 2 with the number of modes. The divergence of the internal energy flows is lower than 10^{-4} W (Eq. (A.10)), and the divergence of the moisture flows is lower than 10^{-4} kg/s (Eq. (A.5)).

In addition, it should be mentioned that the PGD resolution is not incremental. Unlike in classical resolution procedures, there is no difference between time and space coordinates. The solution is assumed to be a space and time separated representation. The field of interest is directly computed for the entire simulation period even if the considered problem is transient.

Considering the low variations of the fields, the time step could have been chosen larger. The time step of the PGD was voluntary chosen very small (10 s) in order to illustrate that the separated representation allows to solve problem of large time domain with very fine time discretisation without increasing significantly the computational time or influencing the accuracy of the solution. The influence of the time step dt (and therefore the number N_t) on the accuracy of the solution is illustrated in Fig. 7(a) and (b). The relative difference is calculated with the PGD solution for a time step of 10 s. It can be noticed that the relative difference is around 10^{-3}% for temperature and vapour pressure. The choice of a larger time step (1 h) has no influence on the accuracy of the PGD solution. It can be noted that PGD resolution allows to consider an adaptive time step as referenced in [49,50].

The concept of numerical complexity is based on [51] and defined as the evolution of the computational time of a numerical algorithm as a function of the degree of freedom of the problem. The degree of freedom of a problem corresponds to its numbers of unknowns. Within the PGD framework, the computational cost is not increased significantly when adding extra coordinates (here space) or the very fine time discretisation because space and time problems are solved separately. Actually, due to the separated representation of the solution, the computational complexity between the large original model (LOM) and the PGD reduced order model (PGD ROM), scales with:

$$\frac{\text{PGD}\quad\text{ROM}}{\text{LOM}} = \frac{M \times (N_z + N_t)}{N_z \times N_t} \simeq \frac{M}{N_z} \tag{4}$$

considering that $N_z \ll N_t$. This computational ratio depends on the choice of the scheme (explicit, implicit, etc.), on the time step (fixed, adaptive, etc.), on the methods used for inversion of matrices, etc. However, it is interesting to point out that the numerical complexity increases linearly for the PGD method, whereas increases exponentially for classic methods (LOM) of resolution of the problem. Thus, the PGD model provides an advantageous numerical gain scaling with the number of zones N_z. Therefore, this gain might be valuable for large buildings composed of many zones. For the case study, following Fig. 6, 3 modes are needed to reach an accurate solution. Thus, the computational cost is about 0.6. For a larger building, considering 20 zones, the computational cost would value 0.15. In addition, for a fixed number of zones, Fig. 7(c) gives the variation of the CPU time for both models (PGD ROM and LOM) as a function of the time step dt (and thus N_t). The evolution of the computational complexity of both algorithms can be evaluated. The computational complexity of the LOM increases more than one of

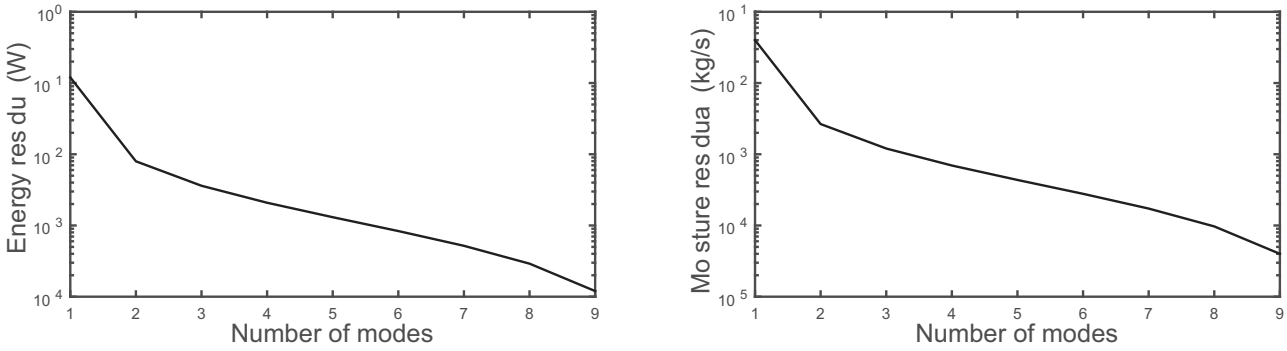

(a) Energy residual (b) Moisture residual

Fig. 6. Evolution of the residual with the number of modes.

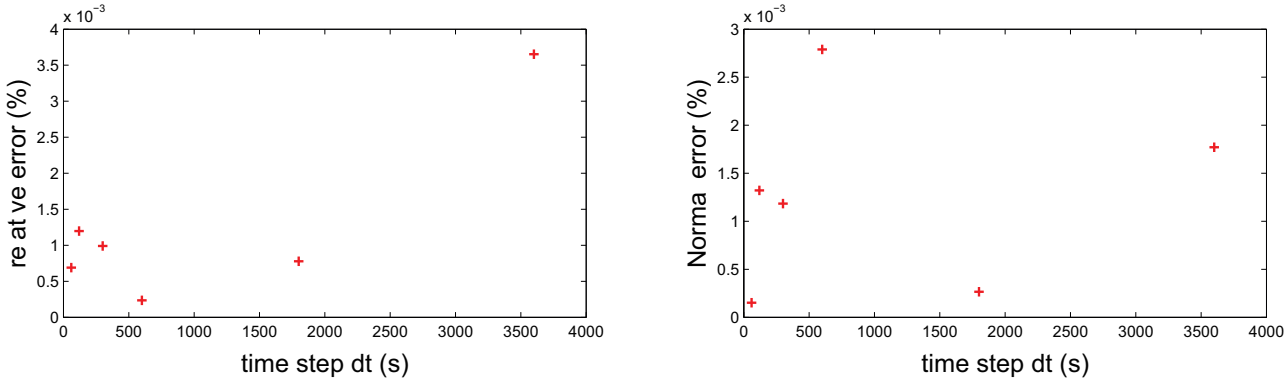

(a) Temperature (b) Presure

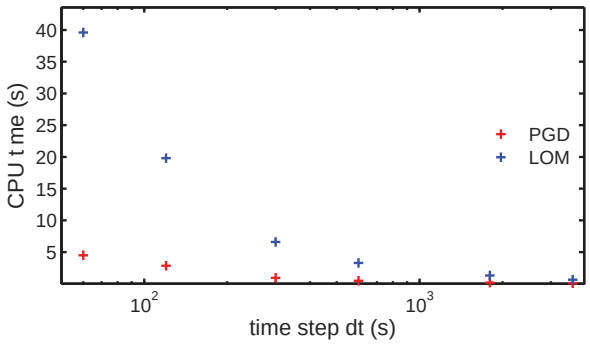

(c) CPU

Fig. 7. Evolution of the relative error for temperature (a), vapour pressure (b) and CPU time (c) as a function of the time step *dt* for the case study of Section 3.

the PGD ROM as a function of the degree of freedom N_t. Differences between the two resolutions are synthesised in Table 2.

4. Model reduction technique for the parametric building multizone model

The previous section illustrated, within the PGD framework, how the local problems of each zone can be transformed into a global problem by introducing an extra coordinate. The advantage is that PGD resolution enables computational savings to solve the problem. In this section, we are interested in more complex problems, based on Problem 1, stemming from parametric considerations. For instance, if one wishes to assess the behaviour of a building for N_{param} parameters (as types of climates, of ventilation flow rates, number of occupants, etc.), Problem 1 has to be solved a number of times equal to the total number of parameters N_{param}. This resolution has therefore a high numerical cost.

As illustrated in many studies reported in the literature [37,45,52–54] as well as in Section 3, the PGD method makes it possible to consider any extra coordinate of the problem and therefore to easily solve parametric problems. In [37,52,54], the heat transfers is calculated as a function of the thermal conductivity parameter. In [45], the Navier–Stokes equation is solved considering different Reynolds numbers. In [53], the epidemiology modelling is considered as a function of the initial conditions.

In this section, it is proposed to apply this feature in order to improve numerical savings on the building multizone model. The aim is to consider the behaviour of a building as a function of

Table 2
Comparison of large original model and PGD reduced order model for computing the solution to Problem 1.

Model	LOM	PGD ROM
Equation[a]	$S\cdot\frac{\mathrm{d}\Theta_z}{\mathrm{d}t}=\Phi_z$ for $z\in\{1,\ldots,N_z\}$	$S\cdot\frac{\mathrm{d}\Theta}{\mathrm{d}t}=\Phi$
Fields	$\Theta_z(t)$ for $z\in\{1,\ldots,N_z\}$	$\Theta(z,t)$
Resolution of the problem	Explicit Euler scheme $\frac{\mathrm{d}\Theta_z}{\mathrm{d}t}\simeq\frac{\Theta_z(t+dt)-\Theta_z(t)}{dt}$	Finite sum representation $\Theta(z,t)=\sum_{m=1}^{M}F^m(z)G^m(t)$
Computational complexity	$N_z\times N_t$	$M\times(N_z+N_t)$
Computational costs[b]	1	$\frac{M}{N_z}$
Values for the case study ($M=3$ and $N_z=5$)	1	0.6
Values for large buildings ($M=3$ and $N_z=20$)	1	0.15

[a] Corresponds to a simplified notation of Problems 1 and 2.
[b] Considering that $N_t\gg N_z$.

different types of climates and ventilation of flow rates. Thus, a climate and ventilation rate parametric problem is defined as:

Problem 3. Find $T(z,t,v,c):\Omega=\Omega_z\times\Omega_t\times\Omega_v\times\Omega_c\longrightarrow\mathbb{R}$ and $P(z,t,v,c):\Omega=\Omega_z\times\Omega_t\times\Omega_v\times\Omega_c\longrightarrow\mathbb{R}$

$$\begin{bmatrix}s_{11}&s_{12}\\s_{21}&s_{22}\end{bmatrix}\begin{bmatrix}\frac{\mathrm{d}T}{\mathrm{d}t}\\\frac{\mathrm{d}P}{\mathrm{d}t}\end{bmatrix}=\begin{bmatrix}q\\g\end{bmatrix}\quad\text{in }\Omega \tag{i}$$

$$\begin{bmatrix}T&P\end{bmatrix}^T=\begin{bmatrix}T_0&P_0\end{bmatrix}^T\quad\text{Initial condition at } t_0 \tag{ii}$$

With v and c coordinates representing the ventilation flow rate of the building and the outside climate (temperature and vapour pressure), respectively. They impact each balance equation with source terms q and g, as detailed in Appendix A. Domains Ω_z, Ω_t, Ω_v and Ω_c are discretised; respectively N_z, N_t, N_v and N_c their number of elements. Problem 3 is a N_c-climate and N_v-ventilation flow rate parametric problem. Its PGD solution is approximated as:

$$T(z,t,v,c)=\sum_{i=1}^{M}F_1^i(z)F_2^i(t)F_3^i(v)F_4^i(c) \tag{5a}$$

$$P(z,t,v,c)=\sum_{i=1}^{M}G_1^i(z)G_2^i(t)G_3^i(v)G_4^i(c) \tag{5b}$$

4.1. Case study

As in previous section, a simple study is now considered to highlight the features and advantages of the model order reduction. The building defined in Section 3.1 is considered. However, instead of considering one climate and one ventilation rate, $N_c=8$ climatic zones and $N_v=10$ flow rates are studied. The climatic zones correspond to the 8 French climatic standards given in [47] and defined as:

$$c=\begin{bmatrix}H1a&H1b&H1c&H2a&H2b&H2c&H2d&H3\end{bmatrix} \tag{6}$$

Climatic data $H1a$ represents a relatively cold climate in the North and $H3$ a warm Mediterranean climate in the South. They define the outside conditions for temperature and vapour pressure as given in Fig. 8 for 3 climatic data.

Ten values of ventilation rate are considered for zones 2 and 4, decreasing from 45 m^3/h to 4.5 m^3/h:

$$v=\begin{bmatrix}45&40.5&36&31.5&27&22.5&18&13.5&9&4.5\end{bmatrix} \tag{7}$$

The first value corresponds to a French standard value for a family house and the last value corresponds to a deteriorated fan.

As described in Section 3.1, all zones are heated and zone 2 and 4 have a daily vapour source. The initial conditions are $T=0\,^\circ$C and $RH=0.3$. Simulation were carried out for one year with a time step of 10 s.

4.2. Results and discussion

4.2.1. Physical analysis

For readability purposes, only 3 solutions are plotted (out of 8 or 10). The main interest here is to verify the physical behaviour of the results given by the PGD reduced order model.

Fig. 9 gives the change in the daily average temperature and vapour pressure in zone 1 for the standard ventilation rate ($v=45$ m^3/h), for 3 different climatic data. It illustrates the solution to the parametric Problem 3 when the ventilation rate is fixed. As climatic data $H3$ corresponds to a warm Mediterranean climate (see Fig. 8), the outside temperature is higher than other zones. During the summer period ($t=200$ days), outside temperature is high and heats the building. This explains why the temperature is higher for climatic data $H3$ than for data $H1a$ or $H2a$ in Fig. 9(a). Same observations can be done for the vapour pressure in Fig. 9(b), as the vapour pressure in climatic data $H3$ is higher than others (see Fig. 8).

Fig. 10 illustrates the impact of the ventilation rate for zone 2, when the climatic data is fixed. In addition, the heat and vapour flow extracted by ventilation in zone 2 as a function of the flow rate are given in Fig. 11. With a low ventilation flow rate, the temperature and vapour pressure are significantly higher than for higher flow rate, as shown in Fig. 10. It is in accordance with observations in Fig. 11. The heat and mass flows extracted from the zone are higher for higher flow rates. Fig. 11 shows that the flows extracted are negative during winter (0–130 days). Not surprisingly, the building looses heat energy and water mass is increasing with the ventilation rate. During the summer, the heat flow is positive and the building is gaining energy.

As a complement, for all ventilation rates and all climatic data, percentage of occurrences when temperature and moisture content in air are higher than T_{limit} and w_{limit} are calculated:

$$\text{occurrences for temperature}=\frac{\int_{\Omega_t}\max\left(0,\frac{T-T_{limit}}{|T-T_{limit}|}\right)dt}{\int_{\Omega_t}dt} \tag{8a}$$

$$\text{occurrences for moisture}=\frac{\int_{\Omega_t}\max\left(0,\frac{w-w_{limit}}{|w-w_{limit}|}\right)dt}{\int_{\Omega_t}dt} \tag{8b}$$

with $T_{limit}=23\,^\circ$C and w_{limit} the moisture content calculated for a relative humidity of 80% and the given temperature of the zone. These limits illustrate situation of discomfort and possible mould growth in the building. Results of occurrences are given in Fig. 12.

Fig. 12 give an example of post-analysis of the PGD solution of the parametric Problem 3. The behaviour of the building is studied for all the climates and all ventilation rates. In zone 1, situation of high temperature is noticed for low ventilation rates and warm climatic data. For the moisture content, it can be noticed that occurrences increase with small ventilation rates. Data $H2b$ presents high values of occurrences as it corresponds to a climatic data with high moisture content (frequent precipitations).

The main purpose of this paragraph was to illustrate that PGD reduced order model enables to compute easily all solutions of the parametric Problem 3. Therefore, the post-treatment of results was simplified. Further analysis could be done using more precise models such as Fanger's model for thermal comfort [55], *VTT* model

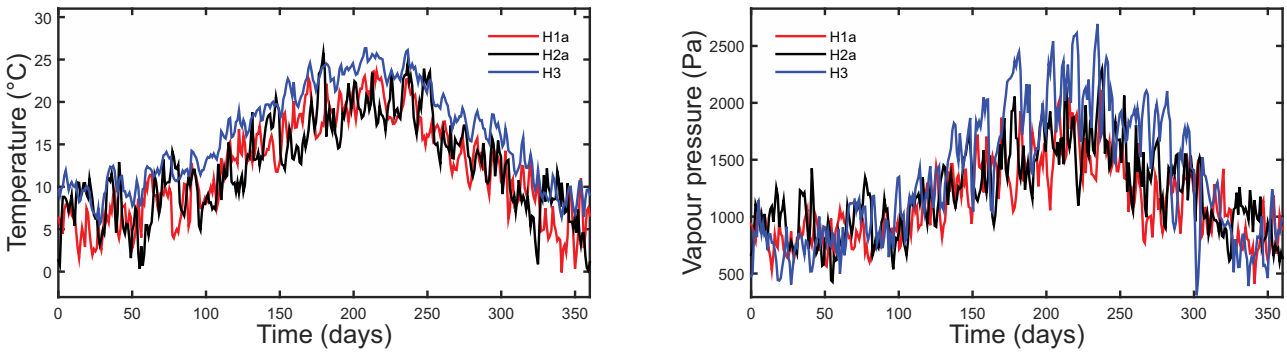

(a) (b)

Fig. 8. Daily averaged outside temperature and vapour pressure for 3 climatic data.

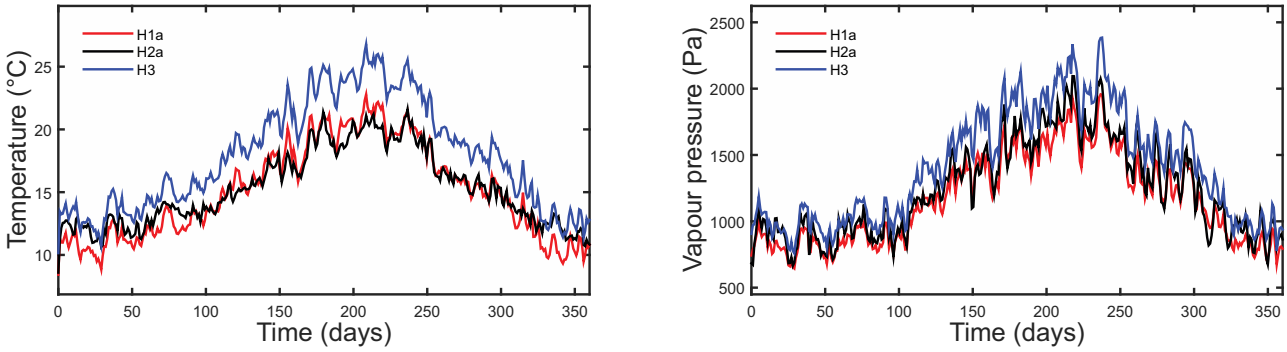

(a) zone 1 (b) zone 1

Fig. 9. Daily averaged temperature and vapour pressure as a function of the climatic data, for $v = 45\,\mathrm{m}^3/\mathrm{h}$.

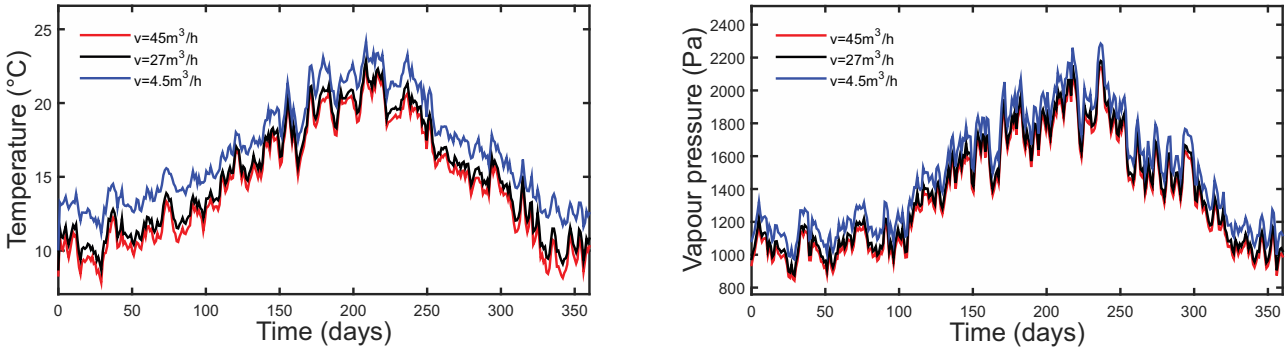

(a) (b)

Fig. 10. Daily averaged temperature and vapour pressure in zone 2 as a function of the ventilation rate for climatic data *H*1*a*.

for mould growth [56] or analysing the energy demand for space heating.

4.2.2. Main features of numerical resolution

6 modes were sufficient to compute the PGD solution. For this number, the divergence of the residual energy flows is lower than 10^{-2} W (Eq. (A.10)), and than 10^{-2} kg/s for the divergence of the moisture flows (Eq. (A.5)). This condition ensures that the PGD algorithm has converged to the solution of the parametric problem. Table 3 compares numerical features of the implemented PGD reduced order model with a large order model associated to Problem 3. N_z, N_t, N_c and N_v are the number of zones, time step, climatic data and ventilation rates, respectively. Thus, the computational savings between the large original model (LOM) and the PGD reduced order model (ROM) scale with:

$$\frac{\text{PGD}\quad\text{ROM}}{\text{LOM}} = \frac{M \times (N_z + N_t + N_c + N_v)}{N_z \times N_t \times N_c \times N_v} \simeq \frac{M}{N_z \times N_c \times N_v} \tag{9}$$

considering that $(N_z, N_c, N_v) \ll N_t$. Thus, PGD resolution offers an interesting numerical gain scaled with the number of zones N_z, climatic data N_c and ventilation rates N_v. The gain was improved compared to non-parametric Problem 2. PGD features improve computational savings significantly when the complexity of the problem increases. A brief estimation for this test case shows that CPU is divided by 12 with a *AMD Phenom II, Processor 2.99 GHZ, 3.49 Gb RAM*. Furthermore, it can be mentioned that Problem 3 was defined as a climate and ventilation parametric problem.

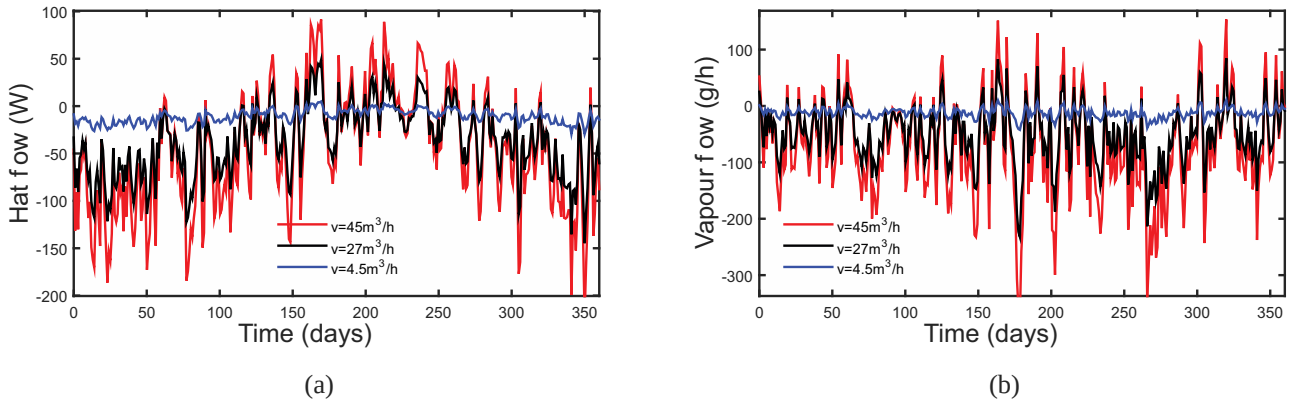

Fig. 11. Daily averaged heat and moisture flow extracted in zone 2 as a function of the ventilation rate for climatic data *H1a*.

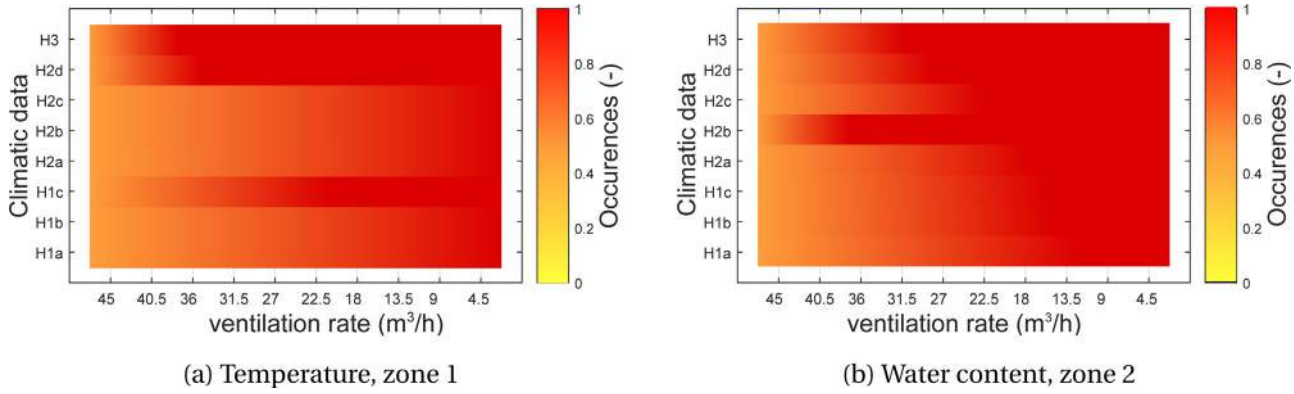

Fig. 12. Percentage of occurrences of high temperature and high moisture content as a function of the climatic data and the ventilation rate.

Table 3
Comparison of the large original model and the PGD reduced order model for computing the solution to the parametric Problem 3.

Model	LOM	PGD ROM
Equation[a]	$S \cdot \frac{d\Theta_{i,j,k}}{dt} = \Phi_{i,j,k}$ for $(i,j,k) \in \{1,\dots,N_z\} \times \{1,\dots,N_v\} \times \{1,\dots,N_c\}$	$S \cdot \frac{d\Theta_k}{dt} = \Phi$
Fields	$\Theta_{i,j,k}(t)$ for $(i,j,k) \in \{1,\dots,N_z\} \times \{1,\dots,N_v\} \times \{1,\dots,N_c\}$	$\Theta(z,t,v,c)$
Resolution of the problem [b]	Explicit Euler scheme $\frac{d\Theta_{i,j,k}}{dt} \simeq \frac{\Theta_{i,j,k}(t+dt)-\Theta_{i,j,k}(t)}{dt}$	Finite sum representation $\Theta(z,t,v,c) = \sum_{m=1}^{M} F^m(z) \cdot G^m(t) \cdot H^m(v) \cdot I^m(c)$
Computational complexity	$\simeq N_z \times N_t \times N_v \times N_c$	$\simeq M \times (N_z + N_t + N_v + N_c)$
Computational costs[c]	1	$\frac{M}{N_z \times N_v \times N_c}$
Values for the case study ($M=6$, $N_z=5$, $N_c=8$ and $N_v=10$)	1	0.03

[a] Corresponds to a simplified notation of Problem 3.
[b] Operator of the PGD solution is actually a Hadamard product, not written to simplify the notation.
[c] Considering that $N_t \gg (N_z, N_c, N_v)$.

It is possible to take into account additional parameters such as the air tightness of the building, incident solar flux, vapour sources, heating sources, etc. More parameters are considered, more the numerical gains due to the use of PGD resolution are significant.

5. Whole building hygrothermal simulation study

5.1. General overview

In the previous section, the PGD model reduction technique was applied to solve a parametric multizone problem. The solution was computed with a reduced computational cost and the behaviour of the building was analysed as a function of the outside climate and the ventilation rate. It is possible to use a very similar approach to progress on hygrothermal simulations of whole buildings, including air zones (multizone model) as well as building envelope (wall model). This section highlights how PGD features can be used within this context. The case studied proposed is based on the works from [57].

Such whole building simulations can be done using a decoupled approach [58], where each model runs sequentially. Each model uses the computed results of the other, as illustrated in Fig. 13. For instance, at time t, the multizone model has to be solved. Solutions $T(t+dt)$ and $P(t+dt)$ are computed as a function of the following coordinates:

- values from the previous time step, as initial conditions in each zone, $T(t)$ and $P(t)$,
- heat and vapour flows represented by source terms $q(t)$ and $g(t)$ computed at time t in each zone,

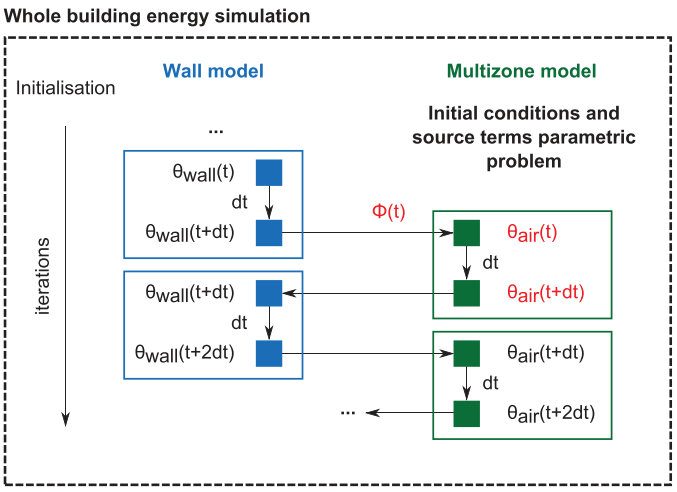

Fig. 13. Association of a multizone model with a wall model to perform a whole-building hygrothermal simulation (θ and respectively Φ are simplified notations; they represent T or P and respectively q or g).

- time-step dt,
- spatial coordinate z representing the number of each zone.

Thus, at each time t, the multizone model has to solve a parametric problem with following coordinates: initial conditions $T_0 = T(t)$, $P_0 = P(t)$ and source terms $q(t)$, $g(t)$. The source terms are different for each zone and therefore depend on spatial coordinate z. Coordinate of the problem must be independent (their variations may not depend of each others). Thus, source terms q and g are decomposed assuming N_z order polynomial expressions $q : (\{a_p\}_{p=1,\dots,N_z}) \in \Omega_a \longrightarrow \mathbb{R}^{N_z}$ and $g : (\{b_p\}_{p=1,\dots,N_z}) \in \Omega_b \longrightarrow \mathbb{R}^{N_z}$, verifying:

$$q(z) = \sum_{p=1}^{N_z} a_p z^{p-1} \tag{10a}$$

$$g(z) = \sum_{p=1}^{N_z} b_p z^{p-1} \tag{10b}$$

This polynomial expression translates relations between the values of the sources in all zones. It should be underlined that this is only a mathematical relation with no physical meaning. In any case, if $p-1 = Z$, this approximation can represent exactly the space (zone) dependence.

Considering this, the PGD method can be used to solve the parametric problem defined as:

Problem 4. Find $T(\{a_p\}_{p=1,\dots,N_z}, T_0, z, t) : \Omega = \Omega_a \times \Omega_{T_0} \times \Omega_z \times \Omega_t \longrightarrow \mathbb{R}$ and $P(\{b_p\}_{p=1,\dots,N_z}, P_0, z, t) : \Omega = \Omega_b \times \Omega_{P_0} \times \Omega_z \times \Omega_t \longrightarrow \mathbb{R}$

$$\begin{bmatrix} s_{11} & s_{12} \\ s_{21} & s_{22} \end{bmatrix} \begin{bmatrix} \dfrac{dT}{dt} \\ \dfrac{dP}{dt} \end{bmatrix} = \begin{bmatrix} \displaystyle\sum_{p=1}^{N_z} a_p z^{p-1} \\ \displaystyle\sum_{p=1}^{N_z} b_p z^{p-1} \end{bmatrix} \quad \text{in } \Omega \tag{i}$$

$$\begin{bmatrix} T & P \end{bmatrix}^T = \begin{bmatrix} T_0 & P_0 \end{bmatrix}^T \quad t = t_0 \tag{ii}$$

Problem 4 is defined for $(z, t, T_0, P_0, \{a_p\}_{p=1,\dots,N_z}, \{b_p\}_{p=1,\dots,N_z}) \in \Omega_z \times \Omega_t \times \Omega_{T_0} \times \Omega_{P_0} \times \Omega_a \times \Omega_b$. The PGD solution is sought as a separated representation of each coordinate:

$$T\left(\{a_p\}_{p=1,\dots,N_z}, T_0, z, t\right) = \sum_{m=1}^{M} \prod_{p=1}^{N_z} F_p^m\left(a_p\right) F_{N_z+1}^m\left(T_0\right) F_{N_z+2}^m(z) F_{N_z+3}^m(t) \tag{11a}$$

$$P_v\left(\{b_p\}_{p=1,\dots,N_z}, P_{v,0}, z, t\right) = \sum_{m=1}^{M} \prod_{p=1}^{N_z} G_p^m\left(b_p\right) G_{N_z+1}^m\left(P_{v,0}\right) G_{N_z+2}^m(z) G_{N_z+3}^m(t) \tag{11b}$$

Solution (11) is a parametric solution. It means that functions $(F_i^m)_{1\le i\le N_z+3}$ and $(G_i^m)_{1\le i\le N_z+3}$ can be calculated only once, at the very beginning of the simulation. These functions can be easily stored and for a given initial condition in $\Omega_{T_0} \times \Omega_{P_0}$ and a given term sources in $\Omega_a \times \Omega_b$, the evolution of the fields can be assessed in all zones by calculating the functional products of functions $(F_i^m)_{1\le i\le N_z+3}$ and $(G_i^m)_{1\le i\le N_z+3}$. Thus, in a whole building energy simulation, the PGD parametric solution (11) can be associated with the wall model within a three-step algorithm:

0. *Initialisation*

(a) Parameters of the simulations are defined: material properties, boundary and initial conditions, etc.

(b) Parametric Problem 4 is solved for a given domain of coordinates $(z, t, T_0, P_0, \{a_p\}_{p=1,\dots,N_z}$ and $\{b_p\}_{p=1,\dots,N_z})$. Functions $(F_i^m)_{1\le i\le N_z+3}$ and $(G_i^m)_{1\le i\le N_z+3}$ are stored.

1. *Wall model* After the first step of initialisation, iterations begin.

(a) The wall model calculates the field of interest in the wall with boundary and initial conditions of the iteration.

(b) Flows exchanged between walls and air zones are calculated using convective coefficients, surface values of the walls and air zone values at the current iteration step.

2. *Multizone model*

(a) Considering the computed flows from the walls and other additional sources or sinks, the source terms q and g influencing heat and moisture balance equations of each zone can be calculated.

(b) Knowing the source terms q and g in each zone for the current iteration, polynomial coefficients $(\{a_p\}_{p=1,\dots,N_z})$ and $(\{b_p\}_{p=1,\dots,N_z})$ that verify (5.1) can be determined.

(c) With the values of the polynomial coefficients $(\{a_p\}_{p=1,\dots,N_z})$ and $(\{b_p\}_{p=1,\dots,N_z})$ and of the initial conditions $T_0 = T(t)$ and $P_0 = P(t)$, the temperature and vapour pressure in all zones can be calculated using the PGD parametric solution (11) computed at the *initialisation* step.

With the computed air temperature and vapour pressure in each zone, the next iteration continues coming back to step 1 to run the wall model.

As stated at the step 2, instead of using a classic solution of a multizone model at each iteration, the solution is computed with the PGD parametric solution.

In the present study, all the algorithms were implemented in MATLAB environment [48] and a application is discussed in the next subsection.

5.2. Case study

The objective is to test the applicability of the innovative solution algorithm presented above to solve problems including hygrothermal transfers in the air zones as well in the building envelopes. For illustrative purposes, the case study is voluntary very simple.

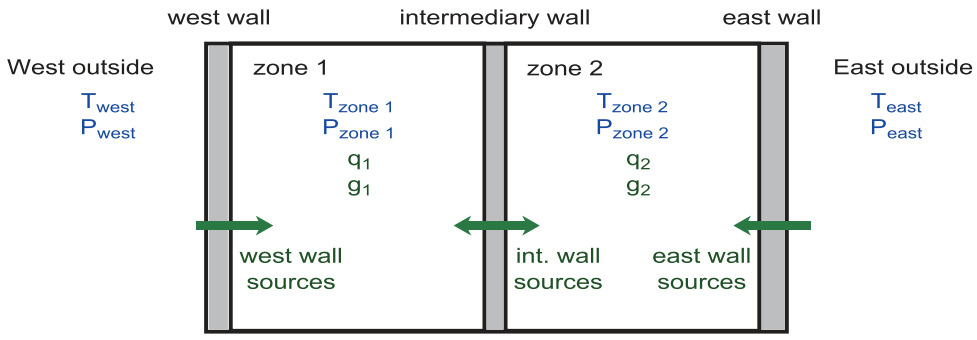

Fig. 14. Schematic view of the case study.

Table 4
Domain of variation of parameters of PGD parametric solution (4).

Coordinates	Minimum	Maximum	Step
Time t (s)	0	360	1
Zones z (m)	1	2	1
Initial temperature T_0 (°C)	0	30	0.01
Initial relative humidity φ_0 (–)	0.1	0.9	0.0001
Heat source term q_1, q_2 (W)	−10	10	0.01
Polynomial coefficient a_2 (W/m)	−20	20	0.01
Polynomial coefficient a_1 (W)	−30	30	0.01
Vapour source term g_1, g_2 (kg/s)	-10^{-2}	10^{-2}	10^{-5}
Polynomial coefficient b_2 (kg/(m s))	$-2\cdot10^{-2}$	$2\cdot10^{-2}$	10^{-5}
Polynomial coefficient b_1 (kg/s)	$-3\cdot10^{-2}$	$3\cdot10^{-2}$	10^{-5}

It considers a building with two 9 m^3 zones. Each zone has one outside wall (see Fig. 14) (East and West) and an intermediary shared wall. Each wall is 2 cm thick with a surface area of 3 m^2. They are composed of the same material, wood fibreboard, whose properties are given in Appendix C. Other bounding surfaces are considered adiabatic and vapour tight. To evaluate the use of the PGD parametric solution, no additional sources or sinks are considered. Thus, there is no heating, ventilation, infiltrations or vapour sources taken into account. The energy and moisture balances in the zone are only modified by flow coming from the 3 walls: q_1 and g_1 for zone 1 and q_2 and g_2 for zone 2. Temperature and vapour pressure in the wall are calculated in 1-dimension with a wall model detailed in [25] and summarised in Appendix C. Heat and vapour flow from walls are calculated following Eqs. (A.7) and (A.11) given in Appendix A and using following heat and moisture convective coefficient: $\alpha = 30\,W/m^2/K$ and $\beta = 3\cdot10^{-7}$ (s/m) for outside western wall and, $\alpha = 8\,W/m^2/K$ and $\beta = 1\cdot10^{-8}$ (s/m) for all others. Initial conditions for walls and zones are $T = 15\,°C$ and $P = 682$ Pa. Boundary conditions are constant $T = 25\,°C$ and $P = 2532$ Pa for western side, and $T = 15\,°C$ and $P = 682$ Pa for eastern side.

For two zones, the expressions of source terms q and g are first-order polynomials:

$$q(z) = a_1 + a_2 z \tag{12a}$$

$$g(z) = b_1 + b_2 z \tag{12b}$$

Problem 4 is defined for 2 zones. The domains of variation of each coordinates are given in Table 4. The accuracy of the temperature and pressure calculated by the parametric solution depends on the mesh of each domain. Thus, a sufficiently fine mesh is considered in each parametric domain. The mesh chosen ensure to calculate the field with a precision of 0.01 °C for temperature and 0.1 Pa. At the *initialisation* step, Problem 4 is solved for a period of 360 s. The PGD parametric solution contains $M = 7$ modes. For this number of modes, the divergence of the internal energy flows is lower than 10^{-2} W (Eq. (A.10)), and the divergence of the moisture flows is lower than 10^{-2} kg/s (Eq. (A.5)). The PGD parametric solution is:

$$T(a_1, a_2, T_0, z, t) = \sum_{m=1}^{7} F_1^m(a_1) F_2^m(a_2) F_3^m(T_0) F_4^m(z) F_5^m(t) \tag{13a}$$

$$P\left(b_1, b_2, P_{v,0}, z, t\right) = \sum_{m=1}^{7} G_1^m(b_1) G_2^m(b_2) G_3^m(P_{v,0}) G_4^m(z) G_5^m(t) \tag{13b}$$

The temperature and vapour pressure in the building (walls and zones) are modelled for a period of 24 h. Since the PGD parametric solution has been computed for a period of 360 s, the time step of the iterations is $dt = 360$ s. The results are compared with two other models. The first one is a large original model used to solve heat and moisture balance (Problem 1 in each zone. This model is coupled with the same wall model detailed in [25]. The second one is the commercial and validated model *WUFI plus* [3].

5.3. Results and discussion

5.3.1. Physical analysis

To perform a physical analysis of the innovative solution algorithm for the case study presented, Fig. 15 shows the temperature and vapour pressure in both zones over time for different modelling approaches. The heat and mass flux entering in each zone are compared in Fig. 16.

As illustrated in Figs. 15 and 16, there is a very good agreement of the PGD parametric solution with the large original model. The PGD parametric solution agrees also well with the *WUFI plus* commercial model. Temperature and vapour pressure are slightly lower and higher respectively, for the *WUFI plus* results. These observations can be explained by the slight differences of heat and mass flux between the two models showed on Fig. 16. Slight differences between both models might come from the description of the Problem 1, particularly from the values of the physical constants. However, relative differences are less than 0.1% for vapour pressure and 0.05% for temperature between the *WUFI plus* and PGD parametric solutions. Considering these results, the PGD parametric solution succeeds in representing the temperature and vapour pressure in both zones. The temporal variations and the amplitude of the hygrothermal fields are accurately represented. There is a delay in the increase of temperature in zones 1 and 2. Vapour pressure in these zones first decreases due to coupled phenomena. Then it increases as moisture flux from western wall increases. The difference in dynamics between heat and moisture phenomena should also be noted. Heat flows change faster than moisture flow.

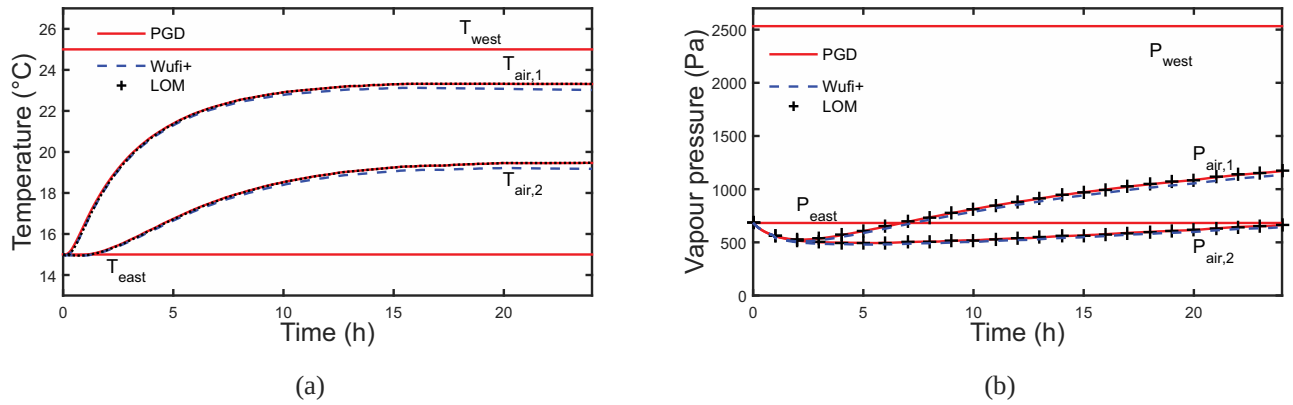

(a) (b)

Fig. 15. Temperature (a) and vapour pressure (b) in both zones for 3 different modelling approaches: PGD parametric solution (red line), large original model (DF black dots), *WUFI plus* modelling (blue marks). (For interpretation of the references to colour in this figure legend, the reader is referred to the web version of this article.)

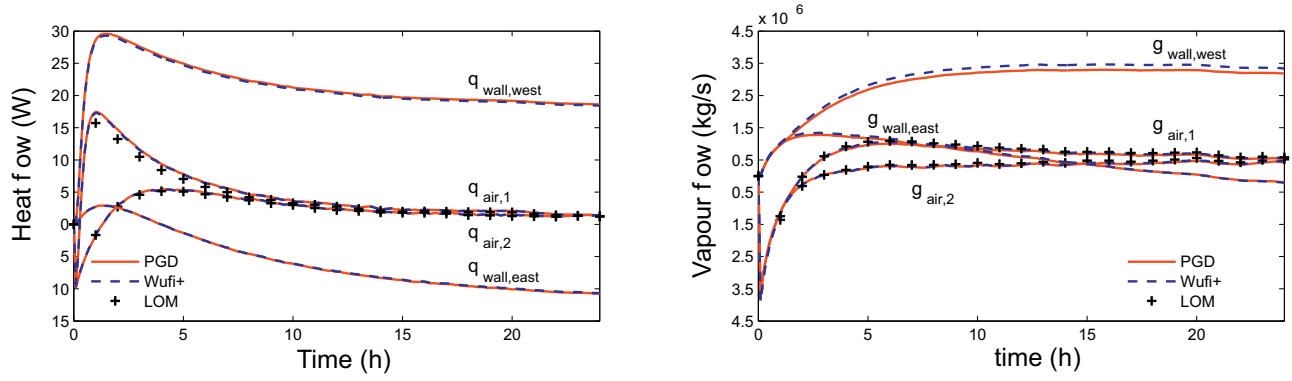

(a) (b)

Fig. 16. Heat (a) and vapour (b) flow entering in both zones for 3 different modelling approaches: PGD parametric solution (red line), large original model (DF black dots), *WUFI plus* modelling (blue marks). (For interpretation of the references to colour in this figure legend, the reader is referred to the web version of this article.)

5.3.2. Main features of numerical resolution

To illustrate precisely the use of the PGD parametric solution, Fig. 17 shows time evolution of temperature and vapour pressure for both zones for time interval $t \in [1; 1.1]$ h. It is the results of particularising the PGD parametric solution and, as mentioned before, there is no resolution of equations to calculate the system evolution. At $t = 1$ h, the heat and mass flows values in zones 1 and 2 are:

$$q_1 = 17.4741 \quad (\mathrm{W}) \quad g_1 = -1.135 \cdot 10^{-6} \quad (\mathrm{kg/s})$$
$$q_2 = -1.7396 \quad (\mathrm{W}) \quad g_2 = -1.1328 \cdot 10^{-6} \quad (\mathrm{kg/s})$$

With this, polynomial coefficients a_1, a_2, b_1 and b_2 are calculated with Eq. (5.1):

$$a_1 = 17.4741 \quad [\mathrm{W}] \quad b_1 = -1.135 \cdot 10^{-6} \quad (\mathrm{kg/s})$$
$$a_2 = -19.2137 \quad [\mathrm{W}] \quad b_2 = 2.5 \cdot 10^{-9} \quad (\mathrm{kg/s})$$

The conditions in zones 1 and 2 at $t = 1$ h are considered as initial conditions in the PGD parametric solution:

$$T_{0,1}(t = 1h) = 16.6 \ ^\circ\mathrm{C} \quad P_{0,1}(t = 1h) = 559.5 \ \mathrm{Pa}$$
$$T_{0,2}(t = 1h) = 14.9 \ ^\circ\mathrm{C} \quad P_{0,2}(t = 1h) = 558.78 \ \mathrm{Pa}$$

With coordinates $(a_1, a_2, b_1, b_2, T_{0,1}, T_{0,2}, P_{0,1}, P_{0,2})$ it is possible to calculate how temperature and vapour pressure evolve in both zones, over 360 s (for $t \in [1; 1.1]$h) from the functional products of functions $(F_i^m)_{\{1\le i\le 5\},\{1\le m\le 7\}}$ and $(G_i^m)_{\{1\le i\le 5\},\{1\le m\le 7\}}$ pre-calculated in the PGD parametric solution (11) at the *initialisation* step. The fields are calculated using:

for zone 1 :

$$T\left(a_1, a_2, T_{0,1}, z = 1, t\right) = \sum_{m=1}^{7} F_1^m(a_1) F_2^m(a_2) F_3^m(T_{0,1}) F_4^m(z) F_5^m(t)$$

for zone 2 :

$$T\left(a_1, a_2, T_{0,2}, z = 2, t\right) = \sum_{m=1}^{7} F_1^m(a_1) F_2^m(a_2) F_3^m(T_{0,2}) F_4^m(z) F_5^m(t)$$

for zone 1 :

$$P\left(b_1, b_2, P_{0,1}, z = 1, t\right) = \sum_{m=1}^{7} G_1^m(b_1) G_2^m(b_2) G_3^m(P_{0,1}) G_4^m(z) G_5^m(t)$$

for zone 2 :

$$P\left(b_1, b_2, P_{0,2}, z = 2, t\right) = \sum_{m=1}^{7} G_1^m(b_1) G_2^m(b_2) G_3^m(P_{0,2}) G_4^m(z) G_5^m(t)$$

The parametric solution is available for the domain variation of parameters: zone z, initial temperature T_0, initial vapour pressure P_0, heat term sources q_1, q_2 and vapour term sources g_1, g_2 defined in Table 4. As illustrated in Fig. 16, the domains of variation of q and g are not violated.

Another interesting feature of the PGD resolution is highlighted here. In a whole building energy simulation, instead of solving the multizone problem at each iteration as a function of the initial condition and the source terms, an accurate parametric solution is calculated. It avoids solving the multizone equations at each

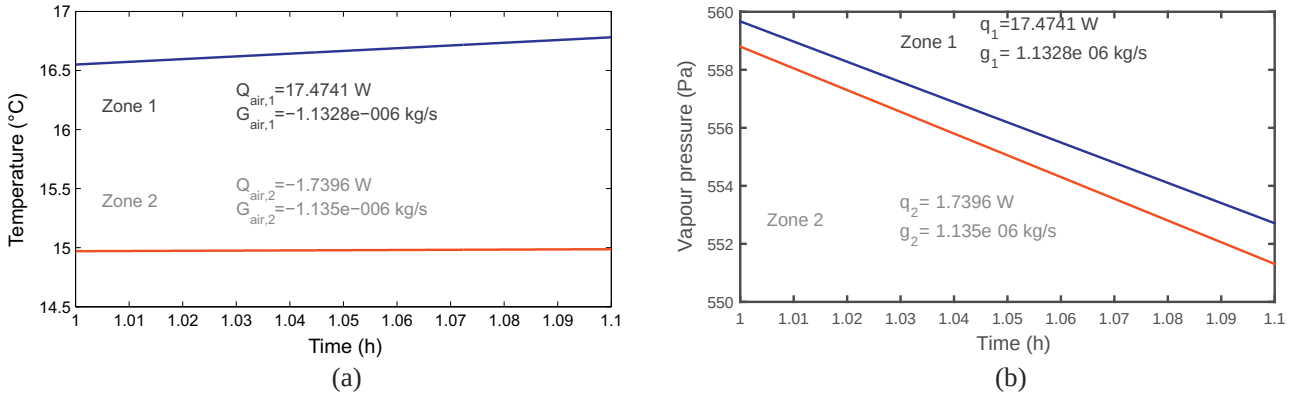

Fig. 17. Temperature (a) and vapour pressure (b) in both zones for $t \in [1; 1.1]$ h, calculated with the PGD-based parametric solution.

Table 5
Comparison of large original model and the PGD parametric solution for computing the solution to the multizone problem.

Model	LOM	PGD parametric solution
Equation[a]	$S \cdot \frac{d\Theta_k}{dt} = \Phi_k \text{ for } (k) \in \{1, \ldots, N_z\}$	$S \cdot \frac{d\Theta_k}{dt} = \Phi$
Fields	$\Theta_k(t) \text{ for } (k) \in \{1, \ldots, N_z\}$	$\Theta(a_1, \ldots, a_{Nz}, T_0, z, t)$
Resolution of the problem [b]	Explicit Euler scheme $\frac{d\Theta_{i,j,k}}{dt} \simeq \frac{\Theta_{i,j,k}(t+dt)-\Theta_{i,j,k}(t)}{dt}$	None, calculation of functional products $\Theta\left(a_1, \ldots, a_{Nz}, \Theta_0, z, t\right) = \sum_{m=1}^{M} \prod_{p=1}^{N_z} F_p^m(a_p) F_{N_z+1}^m\left(\Theta_0\right) \cdot F_{N_z+2}^m(z) F_{N_z+3}^m(t)$
Computational complexity	$N_z \times N_t$	$\epsilon \ll 1$
Computational costs	1	$\epsilon \ll 1$
Values for the case study	1	0.02

[a] Corresponds to a simplified notation of Problem 3.
[b] Operator of the PGD solution is actually a Hadamard product, not written to simplify the notation.

iteration. Functions $(F_i^m)_{\{1\leq i\leq 5\},\{1\leq m\leq 7\}}$ and $(G_i^m)_{\{1\leq i\leq 5\},\{1\leq m\leq 7\}}$ are stored and then the dynamic evolution of the field can be calculated. Within a classical discretisation framework, storing such solutions depending on many parameters is an arduous task. Actually, one must solve many problems (one for each parameter) and of course store all the solutions related to each parameter choice. Obviously, exploring the whole parametric space results is impossible when the number of parameters involved in the model increases.

The calculation of the PGD parametric solution allows substituting the many solutions with simple particularisation of the general parametric solution. The multizone reduced order model, proposed here as a parametric solution, substantially reduces the computational costs. A brief estimation for this test case shows that computational time is divided by 50 with a *AMD Phenom II, Processor 2.99 GHZ, 3.49 Gb RAM*. To appreciate the computational gains, Table 5 compares the differences between the PGD parametric solution, the PGD resolution and the large original model for a 2 zone case study.

For this case study, the PGD parametric solution was created for 2 zones. Whatever the number of zones considered N_z, a polynomial form can be adopted for the expression of q and g. The polynomial coefficients can be integrated into the construction of the PGD parametric solution. Such parametric solutions can be used for multizone modelling for any number of zones N_z. The computational savings increase with the numbers of zones considered, as mentioned in Section 3.2.

6. Conclusion

Proper Generalised Decomposition for solving heat and moisture multizone modelling was proposed in the present paper as an innovative method for solving problems from building physics. As shown in Section 3, the time evolution and the amplitude of hygrothermal fields are perfectly and accurately represented. The PGD resolution is valuable in that local problems in each zone are transformed into a global problem of higher dimensionality. Instead of solving N_z equations for all N_z zones for N_t time steps, one global equation is solved only once to calculate the field of interest in all zones and at all time steps simultaneously. Another interesting feature is that this method is not incremental. It can calculate how the fields evolves over time in transient models. Furthermore, the numerical complexity increases linearly for the PGD method, whereas increases exponentially for classic methods (LOM) of resolution of the problem. Consequently, very fine time discretisation can be considered without important impact on the computational efficiency.

The second advantage of the PGD method is that it can solve parametric problems. The PGD resolution can integrate any extra coordinate of the problem considered. Due to the separated representation of the solution, the construction and the storage of the parametric solution are very fast and easy, even if many parameters are considered. Two interesting illustrations of this feature were put forward in the present paper. In Section 4, a climate data and ventilation flow rate parametric multizone problem was solved using the PGD model reduction technique. The behaviour of building zones was analysed as a function of these parameters. Values of interest were accurately calculated and the computational complexity of the problem was reduced.

In Section 5, another parametric problem was studied: a general parametric solution of multizone problem was computed as a function of the initial condition and the source terms in each zone. Then, this parametric solution was coupled with wall models to perform a whole building energy simulation. At each iteration, instead of solving the multizone problem, the general parametric solution was particularised to calculate the temperature and vapour pressure in each zone. Compared to the large original model, the PGD

parametric solution provides considerable computational savings. In addition, the model represents accurately the temperature and vapour pressure in the different zones.

These results are encouraging for future use of PGD method in whole building hygrothermal simulation. Such reduced order models for walls could be coupled with the parametric solution presented in the present paper, to perform fast and accurate whole building hygrothermal simulations.

Acknowledgements

The authors acknowledge the French National Research Agency (ANR) for funding this work through its Sustainable Buildings and Cities programme (Humibatex project No. ANR-11-BVD).

Appendix A. Heat and moisture multizone modelling for buildings

A.1. Moist air

The vapour mass m_v contained in a volume of moist air V is related to the total mass of dry air by following equation:

$$m_v = w m_a = w \rho_a V \tag{A.1}$$

wih w the ratio between the vapour mass and dry air mass for the volume V, m_a dry air mass and ρ_a dry air density.

The ratio w is related to vapour pressure P and total pressure P_a of the volume by:

$$w = \frac{M_v}{M_a} \frac{P}{P_a - P} \tag{A.2}$$

Given that $P_a \gg P$, we assumed that:

$$w \simeq \frac{M_v}{M_a} \frac{P}{P_a} \tag{A.3}$$

Thus, with (A.1) and (A.3), we obtain:

$$m_v = \frac{M_v}{M_a} \frac{\rho_a V}{P_a} P \tag{A.4}$$

A.2. Mass balance in air volume

Moist air zone typically (one room or group of rooms) is considered perfectly mixed. The water vapour mass balance for the control volume V considers vapour sources or sinks due to:

1 Vapour flow transported by air flow (advection) g_a. Flows due to ventilation systems, to infiltrations or to transfers between zones belong to this group.
2 Additional sources or sink due to occupants metabolism and activities, plants, etc. g_s.
3 Mass convection from bounding walls g_w.

Vapour diffusion in air and buffering by furniture, etc. are ignored. Thus, the mass balance of volume V is expressed as:

$$\frac{\mathrm{d}m_v}{\mathrm{d}t} = g_a + g_w + g_s \tag{A.5}$$

knowing (A.4), Eq. (A.5) becomes:

$$\frac{M_v}{M_a} \frac{\rho_a V}{P_a} \frac{\mathrm{d}P}{\mathrm{d}t} = g_a + g_w + g_s \tag{A.6}$$

A.2.1. Vapour sources

Occupants and their activities, animals, plants, etc. produce vapour inside zones and influence the vapour balance of each zone. Moon gives a detailed list of potential vapour sources and their values [59]. The term g_s in Eq. (A.6) is therefore a given parameters. It is an instationnary parameter specific for each zone of the building.

A.2.2. Convective mass from walls

Convective mass flows from surfaces are calculated by:

$$g_w = \sum_{s=1}^{N_s} \beta_s A_s (P_s - P) \tag{A.7}$$

with

P_s	the vapour pressure at the surface of bounding walls s
β_s	the convective mass transfer coefficient for surface s
A_s	the area of surface s
N_s	the numbers of bounding surfaces

The vapour pressure at the surface of bounding walls P_s is calculated using wall model (see Appendix C).

A.2.3. Vapour flow from advection

Vapour can be transported by moist air transfers between zones through openings or by ventilation systems. For our work, air flows are not modelled and are given as inputs of the problem. The vapour flow due to the air transfer is expressed as:

$$g_a = \sum_{j=1}^{N_z} \dot{m}_{a,j} w_j \tag{A.8}$$

with

w_j	the vapour content of air
$\dot{m}_{a,j}$	the air flow coming from zone$j$
N_z	the total number of zones contributing to balance of the volume V

Flow can be entering or exiting the zone.

A.3. Energy balance of air volume

For a control volume i, the heat balance considers:

1 heat flow transported by air flow (advection) q_a,
2 surface convection at the bounding walls q_w,
3 convective sources of heat q_s.

Energy of the air volume V considers the thermal capacity of air and moisture. The energy balance of the control volume is written:

$$\rho_a C_a V \cdot \frac{\mathrm{d}T}{\mathrm{d}t} + L_v \frac{\mathrm{d}m_v}{\mathrm{d}t} = q_w + q_s + q_a \tag{A.9}$$

which can be expressed as:

$$(C_a + w C_v) \rho_a V \frac{\mathrm{d}T}{\mathrm{d}t} + L_v \frac{M_v}{M_a} \frac{\rho_a V}{P_a} \frac{\mathrm{d}P}{\mathrm{d}t} = q_w + q_s + q_a \tag{A.10}$$

with

ρ_a	the density of dry air
w	the vapour content of air
C_a	the heat capacity of dry air
C_v	the heat capacity of vapour

A.3.1. Heat sources

Several heat sources can be identified within a single overall term source g_s, known as input of the problem. It integrates heat sources:

1 due to occupation of the zone,
2 due to use of electric equipment,
3 due to the building's heating or cooling systems.

A.3.2. Heat convection from walls

Surface convection heat rates at the bounding walls are expressed as:

$$q_w = \sum_{s=1}^{N_s} \alpha_s A_s (T_s - T) + L_v \beta_s A_s (P_s - P) \tag{A.11}$$

with

T_s	the	surface temperature of bounding walls s
α_s	the	convective heat transfer coefficient for surface s
A_s	the	area of surface s
N_s	the	numbers of bounding surfaces
L_v	the	latent heat of evaporation

A.3.3. Heat source from advection

As mentioned above, air flows are not modelled in the present work. This is a given parameter of the problem. The heat source due to air flows coming from other zones is expressed as:

$$q_a = \sum_{j=1}^{N_z} \dot{m}_{a,j} C_a (T_j - T) \tag{A.12}$$

with

C_a	the	heat capacity of
$\dot{m}_{a,j}$	the	air flow coming from zone$j$
N_z	the	total number of zone contributing to balance of the volume V

A.4. Hygrothermal multizone modelling

Considering balance Eqs. (A.6) and (A.10) for one zone, we have:

$$\begin{bmatrix} s_{11} & s_{12} \\ s_{21} & s_{22} \end{bmatrix}_k \begin{bmatrix} \dfrac{\mathrm{d}T}{\mathrm{d}t} \\ \dfrac{\mathrm{d}P}{\mathrm{d}t} \end{bmatrix} = \begin{bmatrix} q \\ g \end{bmatrix} \tag{A.13}$$

Knowing that a building is composed of N_z zones, hygrothermal multizone modelling is defined by following problem: $\forall k = \{1, \ldots, N_z\}$, Find $T_k(t) : \Omega_t \longrightarrow \mathbb{R}$ and $P_k(t) : \Omega_t \longrightarrow \mathbb{R}$

$$\begin{bmatrix} s_{11} & s_{12} \\ s_{21} & s_{22} \end{bmatrix}_k \begin{bmatrix} \dfrac{\mathrm{d}T}{\mathrm{d}t} \\ \dfrac{\mathrm{d}P}{\mathrm{d}t} \end{bmatrix}_k = \begin{bmatrix} q \\ g \end{bmatrix}_k \quad \text{in } \Omega_t \tag{i}$$

$$\begin{bmatrix} T & P \end{bmatrix}_k = \begin{bmatrix} T_0 & P_0 \end{bmatrix}_k \quad \text{Initial condition at } t_0 \tag{ii}$$

with

$$s_{11} = \rho_a C_a V \tag{A.14a}$$

$$s_{12} = L_v \frac{M_v}{M_a} \frac{\rho_a V}{P_a} \tag{A.14b}$$

$$s_{21} = 0 \tag{A.14c}$$

$$s_{22} = \frac{M_v}{M_a} \frac{\rho_a V}{P_a} \tag{A.14d}$$

$$q = q_a + q_w + q_s \tag{A.14e}$$

$$g = g_a + g_w + g_s \tag{A.14f}$$

Appendix B. PGD solution

To explain PGD algorithm, we consider Θ as the field of interest in the whole space (zones)-time domain, verifying:

Problem 5. $\forall (x, t) \in \Omega = \Omega_x \times \Omega_t$, find $\Theta(x, t) : \Omega \longrightarrow \mathbb{R}$

$$C(\Theta) \cdot \frac{\partial \Theta}{\partial t} = \Phi \quad \text{in } \Omega \tag{i}$$

$$\Theta = \Theta_0 \quad \text{Initial condition at } t_0 \tag{ii}$$

For $(x, t) \in \Omega = \Omega_1 \times \Omega_2$, the PGD solution to Problem 5 is sought as a separated representation of time t and space x:

$$\Theta(t, x) \simeq \sum_{i=1}^{M} F^i(t) \cdot G^i(x) \tag{B.2}$$

B.1. Iterative resolution

Solving Problem 5 numerically using the PGD method consists in calculating modes (F^i, G^i) iteratively from $i = 1$ to $i = M$. The first mode (F^1, G^1) is initialised in order to verify the initial and boundary conditions in all zones.

At enrichment step $m < M$, we assume that a former approximation of $\Theta(t, x)$ is known and the new couple $F^{m+1}(t) = R(t)$ and $G^{m+1}(x) = S(x)$ has to be calculated according to:

$$\Theta(t, x) = \sum_{i=1}^{m} F^i(t) \cdot G^i(x) + R(t) \cdot S(x) \tag{B.3}$$

Eq. (B.3) is introduced into Problem 5. Due to the separated representation of the solution Θ for dimensions t and x we have:

$$C \cdot \frac{dR}{dt} \cdot S = \Phi - \sum_{i=1}^{m} C \cdot \frac{dF^i}{dt} \cdot G^i + Res^{m+1} \tag{B.4}$$

Res^{m+1} is a residual because Eq. (B.3) is an approximation of the solution. Before solving Eq. (B.4), the non-linearity of coefficient matrix C must be considered.

B.2. Treating non-linearity

An important problems terms from to the fact that problem (B.4) is non-linear. Capacity matrix C depends on Θ.

In the present work, at iteration $m+1$, the non-linear term $C(\Theta^{m+1}) \cdot \Theta^{m+1}$ is evaluated using the solution from iteration m. Therefore, at each enrichment step $m+1$, matrix C is calculated using previous modes of Θ.

$$C(\Theta^{m+1}) = C\left(\sum_{i=1}^{m} F^i \cdot G^i + R \cdot S\right) \simeq C\left(\sum_{i=1}^{m} F^i \cdot G^i\right) \tag{B.5}$$

Then C is separated by a tensorial product in the space and time directions, using *singular value decomposition*:

$$C(\Theta) = \sum_{j=1}^{n_C} C_t^j(t) \cdot C_x^j(x) \tag{B.6}$$

This decomposition enables us to separate the capacity and diffusion matrices into a component depending on time and another

depending on space. As observed in this study and for the sake of simplicity, n_C is assumed equal to 1. Therefore, Eq. (B.4) becomes:

$$\left(C_t \cdot \frac{dR}{dt}\right) \cdot (C_x \cdot S) = \Phi(x) - \sum_{i=1}^{m} \left(C_t \cdot \frac{dF^i}{dt}\right) \cdot (C_x \cdot G^i) + Res^{m+1} \tag{B.7}$$

B.3. Computing R(t) and S(x)

We are at step m searching for the new couple R and S by solving Eq. (B.4). To compute them, Eq. (B.4) will be successively projected on R and S.

For this, we note:

- $\langle \bullet, \bullet \rangle_{\Omega_1}$ the scalar product in Ω_1,
- $\langle \bullet, \bullet \rangle_{\Omega_2}$ the scalar product in Ω_2.

Eq. (B.4) is projected on S, assuming $\langle Res^{m+1}, S \rangle_{\Omega_2} = 0$ to obtain:

$$\alpha_1 \cdot C_t \cdot \frac{dR}{dt} = \beta_1 + \gamma_1 \tag{B.8}$$

With:

$$\begin{cases} \alpha_1 = \langle S, C_x \cdot S \rangle_{\Omega_2} \\ \beta_1 = \langle S, \Phi \rangle_{\Omega_2} \\ \gamma_1 = -\sum_{i=1}^{m} \langle S, C_x \cdot G^i \rangle_{\Omega_2} \cdot C_t \cdot \frac{dF^i}{dt} \end{cases} \tag{B.9}$$

Eq. (B.4) is now projected on R, assuming $\langle Res^{m+1}, R \rangle_{\Omega_2} = 0$ and gives:

$$\alpha_2 \cdot C_x \cdot S = \beta_2 + \gamma_2 \tag{B.10}$$

With:

$$\begin{cases} \alpha_2 = \langle R, C_t \cdot \frac{dR}{dt} \rangle_{\Omega_1} \\ \beta_2 = \langle R, \Phi \rangle_{\Omega_1} \\ \gamma_2 = -\sum_{i=1}^{m} \langle R, C_t \cdot \frac{dF^i}{dt} \rangle_{\Omega_1} \cdot C_x \cdot G^i \end{cases} \tag{B.11}$$

After theses projections, to solve Eqs. (B.8) and (B.10) an alternating direction fixed-point algorithm is used. The stopping criterion, assuming the algorithm has converged, is:

$$\|R^q - R^{q-1}\|_{\Omega_2} < \epsilon \text{ and } \|S^q - S^{q-1}\|_{\Omega_1} < \epsilon \tag{B.12}$$

where q the index of iteration of the fixed-point algorithm and ϵ is a parameter chosen by user.

B.4. Convergence of global enrichment

R and S have just been computed by a fixed-point algorithm. The PGD basis is enriched, noting $F^{m+1} = R$ and $G^{m+1} = S$ the new modes. The field of interest Θ can be written as:

$$\Theta(t,x) = \sum_{i=1}^{m} F^i(t) \cdot G^i(x) + R(t) \cdot S(x) = \sum_{i=1}^{m+1} F^i(t) \cdot G^i(x) \tag{B.13}$$

The enrichment of the PGD solution stops when the Euclidean norm of the residual $\|Res^M\|_{H^1(\Omega)}$ is assumed negligible with respect to η, a parameter chosen by the user:

$$\|Res^M\|_{\Omega=\Omega_1\times\Omega_2} = \|\sum_{i=1}^{M} \frac{dF^i(t)}{dt} \cdot G^i(x) - \Phi\|_{\Omega} \leq \eta \tag{B.14}$$

Appendix C. Heat and moisture transfer in material

As mentioned in Section 5, more details of the wall models are given in [25]. This appendix gives the main information on the heat and mass transfer model considered.

It is assumed that pores are filled with a liquid phase, composed of liquid water, and a gaseous phase, considered as a mixture of dry air and water vapour. The mass balance of water depends on the moisture flows of the vapour phase. The heat balance takes into account conductive and convective flows. The equations of heat and mass transfer can be expressed as:

$$\int\int\int_V \left(c_{11}\frac{\partial T}{\partial t} + c_{12}\frac{\partial P}{\partial t} - \mathrm{div}\,(d_{11}\mathrm{grad}T + d_{12}\mathrm{grad}P)\right) dV = 0 \tag{C.1a}$$

$$\int\int\int_V \left(c_{21}\frac{\partial T}{\partial t} + c_{22}\frac{\partial P}{\partial t} - \mathrm{div}\,(d_{21}\mathrm{grad}T + d_{22}\mathrm{grad}P)\right) dV = 0 \tag{C.1b}$$

with $\{c_{i,j}\}_{i=1,2,j=1,2}$ and $\{d_{i,j}\}_{i=1,2,j=1,2}$ corresponding to the storage and diffusion properties of the materials, expressed as:

$$\begin{cases} c_{11}(T,P) = \rho_m\,(c_m + c_v w) \\ c_{12}(T,P) = c_v T \xi \\ c_{21}(T,P) = 0 \\ c_{22}(T,P) = \xi \\ d_{11}(T,P) = \lambda \\ d_{12}(T,P) = \delta_v L_v \\ d_{21}(T,P) = 0 \\ d_{22}(T,P) = \delta_v + K_l \frac{\rho_l R_v T}{P} \end{cases} \tag{C.2}$$

Table C.6
Hygrothermal properties of wood fiberboard.

Sorption curve (kg/m^3)	$m = 17.07$, $c = 8.076$, $k = 0.9699$	$w = m \cdot c \cdot \frac{\frac{P}{P_{sat}}}{\left(1-k\cdot\frac{P}{P_{sat}}\right)\left(1-(k-c)\cdot\frac{P}{P_{sat}}\right)}$
Liquid permeability (s)	$K_0 = 1.17 \cdot 10^{-16}$, $a_1 = 0.2449$, $b_1 = 1.339$, $a_2 = -0.2441$, $b_2 = -93.79$	$K_l = K_0 \cdot \left(a_1 \cdot \exp\left(b_1 \cdot \frac{w}{w_0}\right) + a_2 \cdot \exp\left(b_2 \cdot \frac{w}{w_0}\right)\right)$
Vapour permeability (kg/m/s/Pa)	$D_{v0} = 2.61 \cdot 10^{-5}$	$\delta_v = \frac{D_{v0}}{462*T} \cdot (-18.14 \cdot 10^{-4} \cdot w + 1)$
Thermal conductivity (W/(m K))	$\lambda_0 = 0.107$, $b = 0.4747 \cdot 10^{-3}$	$\lambda = \lambda_0 + b \cdot w$
Heat storage (J/m^3/K)	$\rho_0 \cdot c_0 = 1551 \cdot 589$	–

with

$$\begin{array}{ll} \rho_m & \text{the dry density of the material} \\ c & \text{the thermal capacity} \\ \xi = \dfrac{\partial w}{\partial P_v} & \text{the moisture storage coefficient} \\ \lambda & \text{the heat conductivity} \\ \delta_v & \text{the vapour moisture diffusion} \\ K_l & \text{the liquid moisture diffusion} \\ R_v & \text{the perfect gas constant for water} \\ \rho_l & \text{the density of liquid water} \end{array} \tag{C.3}$$

The properties of the material used in Section 5 are given in Table C.6.

References

[1] M. Woloszyn, C. Rode, Tools for performance simulation of heat, air and moisture conditions of whole buildings, Build. Simul. 1 (March (1)) (2008) 5–24.

[2] A. Sasic Kalagasidis, P. Weitzmann, T.R. Nielsen, R. Peuhkuri, C.-E. Hagentoft, C. Rode, The international building physics toolbox in simulink, Energy Build. 39 (June (6)) (2007) 665–674.

[3] Fraunhofer IBP, Wufi, 2005. Available from: http://www.hoki.ibp.fhg.de/wufi/wufi_frame_e.html

[4] A.D. Tran Le, C. Maalouf, K. Cordeiro Mendonça, H. Mai, E. Wurtz, Study of moisture transfer in a double-layered wall with imperfect thermal and hydraulic contact resistances, J. Build. Perform. Simul. 2 (4) (2009) 251–266.

[5] BC Bauklimatik Dresden, Simulation Program for the Calculation of Coupled Heat, Moisture, Air, Pollutant, and Salt Transport. Available from: http://www.bauklimatik-dresden.de/delphin/index.php?ala=en

[6] H.M. Künzel, P. Kiessl, Simultaneous Heat and Moisture Transport in Building Components: One- and Two-dimensional Calculation Using Simple Parameters, Fraunhofer IRB, 1995.

[7] Q. Li, J. Rao, P. Fazio, Development of HAM tool for building envelope analysis, Build. Environ. 44 (May (5)) (2009) 1065–1073.

[8] H. Janssen, B. Blocken, J. Carmeliet, Conservative modelling of the moisture and heat transfer in building components under atmospheric excitation, Int. J. Heat Mass Transf. 50 (March (5–6)) (2007) 1128–1140.

[9] U.S. Department of Energy, Model for Multidimensional Heat, Air and Moisture Conditions in Building Envelope Components, 2011. Available from: http://wwwx.dtu.dk/Centre/bfi/md-ham.aspx

[10] H. Hens, J. Carmeliet, Performance prediction for masonry walls with EIFS using calculation procedures and laboratory testing, J. Build. Phys. 25 (January (3)) (2002) 167–187.

[11] U.S. Department of Energy, Energyplus Energy Simulation Software, 2014. Available from: http://apps1.eere.energy.gov/buildings/energyplus/?utm_source=EnergyPlus&utm_medium=redirect&utm_campaign=EnergyPlus

[12] SEL, TRNSYS, 2012. Available from: http://sel.me.wisc.edu/trnsys/features/features.html

[13] D. Derome, Moisture Occurrence in Roof Assemblies Containing Moisture Storing Insulation and its Impact on the Durability of Building Envelope (Ph.D. thesis), Concordia University, Montreal, Quebec, Canada, October 1999.

[14] R.M. Barbosa, N. Mendes, Combined simulation of central HVAC systems with a whole-building hygrothermal model, Energy Build. 40 (3) (2008) 276–288.

[15] A. Piot, C. Abele, M. Woloszyn, J. Brau, Numerical simulation aided design of an experimental protocol, in: In: Proceedings of the 8th Symposium on Building Physics in the Nordic Countries, vol. 2, Carsten Rode, June 2008.

[16] F. Tariku, K. Kumaran, P. Fazio, Transient model for coupled heat, air and moisture transfer through multilayered porous media, Int. J. Heat Mass Transf. 53 (July (15–16)) (2010) 3035–3044.

[17] M. Steeman, A. Janssens, H.J. Steeman, M. Van Belleghem, M. De Paepe, On coupling 1D non-isothermal heat and mass transfer in porous materials with a multizone building energy simulation model, Build. Environ. 45 (April (4)) (2010) 865–877.

[18] Joe Clarke, Moisture flow modelling within the ESP-r integrated building performance simulation system, J. Build. Perform. Simul. 6 (5) (2013) 385–399.

[19] C. Spitz, M. Woloszyn, C. Buhe, M. Labat, Simulating combined heat and moisture transfer with EnergyPlus: an uncertainty study an comparison with experimental data, in: In: Building Simulation 2013, Proceedings, Chambery, France, International Building Performance Simulation Association (IBPSA), 2013.

[20] G.H. dos Santos, N. Mendes, Simultaneous heat and moisture transfer in soils combined with building simulation, Energy Build. 38 (April (4)) (2006) 303–314.

[21] J. Berger, S. Tasca-Guernouti, M. Woloszyn, C. Buhe, Mould growth damages due to moisture: comparing 1d and 2d heat and moisture models, in: IBPSA 2013, Building Siumlation International Conference, Chambery, France, August 2013.

[22] A. Cornick, S. Maref, P. Mukhopadhyaya, A. Dalgliesh, S. Cornick, W. Maref, P. Mukhopadhyaya, Hygrothermal Performance of Building Envelopes: Uses for 2D and 1D Simulation, NRC Publications Archive.

[23] L.H. Mortensen, M. Woloszyn, C. Rode, R. Peuhkuri, Investigation of microclimate by CFD modeling of moisture interactions between air and constructions, J. Build. Phys. 30 (January (4)) (2007) 279–315.

[24] Masaru Abuku, Hans Janssen, Staf Roels, Impact of wind-driven rain on historic brick wall buildings in a moderately cold and humid climate: Numerical analyses of mould growth risk indoor climate and energy consumption, Energy Build. 41 (1) (2009) 101–110.

[25] J. Berger, M. Chhay, S. Guernouti, M. Woloszyn, Proper generalised decomposition for solving coupled heat and moisture transfers, J. Build. Perform. Simul. (2014), http://dx.doi.org/10.1080/19401493.2014.932012

[26] T. Hong, Y. Jiang, A new multizone model for the simulation of building thermal performance, Build. Environ. 32 (2) (1997) 123–128.

[27] M.M. Gouda, S. Danaher, C.P. Underwood, Low-order model for the simulation of a building and its system, Build. Serv. Eng. Res. Technol. 21 (3) (2000) 199–208.

[28] S.T. Parker, D.M. Lorenzetti, M.D. Sohn, Implementing state-space methods for multizone contaminant transport, Build. Environ. 71 (0) (2014) 131–139.

[29] S.T. Parker, V. Bowman, State-space methods for calculating concentration dynamics in multizone buildings, Build. Environ. 46 (8) (2011) 1567–1577.

[30] S. Goyal, P. Barooah, A method for model-reduction of non-linear thermal dynamics of multi-zone buildings, Energy Build. 47 (0) (2012) 332–340.

[31] P. Ladeveze, Sur une famille d'algorithmes en mécanique des structures, Comptes-rendus des scéances de l'Académie des sciences. Série 2, Mécanique-physique, chimie, sciences de l'univers, sciences de la terre 300 (2) (1985) 41–44.

[32] A. Ammar, B. Mokdad, F. Chinesta, R. Keunings, A new family of solvers for some classes of multidimensional partial differential equations encountered in kinetic theory modelling of complex fluids. Part II: Transient simulation using space-time separated representations, J. Non-Newtonian Fluid Mech. 144 (July (2–3)) (2007) 98–121.

[33] F. Chinesta, P. Ladeveze, E. Cueto, A short review on model order reduction based on proper generalized decomposition, Arch. Comput. Methods Eng. 18 (November (4)) (2011) 395–404.

[34] F. Chinesta, A. Leygue, F. Bordeu, J.V. Aguado, E. Cueto, D. Gonzalez, I. Alfaro, A. Ammar, A. Huerta, PGD-based computational vademecum for efficient design, optimization and control, Arch. Comput. Methods Eng. 20 (March (1)) (2013) 31–59.

[35] F. Chinesta, R. Keunings, A. Leygue, The Proper Generalized Decomposition for Advanced Numerical Simulations: A Primer, Springer International Publishing AG, New York, October 2013.

[36] A. Ammar, F. Chinesta, Circumventing curse of dimensionality in the solution of highly multidimensional models encountered in quantum mechanics using meshfree finite sums decomposition, in: M. Griebel, M.A. Schweitzer (Eds.), Meshfree Methods for Partial Differential Equations IV, number 65 in Lecture Notes in Computational Science and Engineering, Springer Berlin Heidelberg, January 2008, pp. 1–17.

[37] E. Pruliere, F. Chinesta, A. Ammar, On the deterministic solution of multidimensional parametric models using the proper generalized decomposition, Math. Comput. Simul. 81 (December (4)) (2010) 791–810.

[38] A. Ammar, M. Normandin, F. Daim, D. Gonzalez, E. Cueto, F. Chinesta, Non incremental strategies based on separated representations: applications in computational rheology, Commun. Math. Sci. 8 (September (3)) (2010) 671–695, Mathematical Reviews number (MathSciNet): MR2730326; Zentralblatt MATH identifier: 05838595.

[39] H. Lamari, A. Ammar, A. Leygue, F. Chinesta, On the solution of the multidimensional langer's equation using the proper generalized decomposition method for modeling phase transitions, Model. Simul. Mater. Sci. Eng. 20 (January (1)) (2012) 015007.

[40] S. Niroomandi, I. Alfaro, E. Cueto, F. Chinesta, Accounting for large deformations in real-time simulations of soft tissues based on reduced-order models, Comput. Methods Prog. Biomed. 105 (January (1)) (2012) 1–12.

[41] S. Niroomandi, I. Alfaro, D. González, E. Cueto, F. Chinesta, Model order reduction in hyperelasticity: a proper generalized decomposition approach, Int. J. Numer. Methods Eng. 96 (October (3)) (2013) 129–149.

[42] S. Niroomandi, F. Bordeu, I. Alfaro, D. Gonzalez, A. Leygue, E. Cueto, F. Chinesta, Real-time Simulation for Virtual Surgery in a PGD Framework, ASME, July 2012, pp. 247–251.

[43] A. Nouy, O.P. Le Maıtre, Generalized spectral decomposition for stochastic nonlinear problems, J. Comput. Phys. 228 (January (1)) (2009) 202–235.

[44] D. Neron, P. Ladeveze, Proper generalized decomposition for multiscale and multiphysics problems, Arch. Comput. Methods Eng. 17 (December (4)) (2010) 351–372.

[45] A. Dumon, C. Allery, A. Ammar, Proper general decomposition (PGD) for the resolution of Navier–Stokes equations, J. Comput. Phys. 230 (February (4)) (2011) 1387–1407.

[46] M.S. Aghighi, A. Ammar, C. Metivier, M. Normandin, F. Chinesta, Non-incremental transient solution of the Rayleigh–Bénard convection model by using the PGD, J. Non-Newtonian Fluid Mech. 200 (2013) 65–78.

[47] Journal Officiel de la République Française, TH-b-CE, 2012, fascicule TH-u matériaux, arrêté du 18 mai 2011. Available from: http://www.rt-batiment.fr/

batiments-neufs/reglementation-thermique-2012/donnees-meteorologiques.html (18.5.11).
[48] B.W. Bader, T.G. Kolda et al., Matlab Tensor Toolbox, Version 2.5 (available online, 2012-01).
[49] F. Chinesta, A. Ammar, E. Cueto, Proper generalized decomposition of multiscale models, Int. J. Numer. Methods Eng. 83 (8–9) (2010) 1114–1132.
[50] A. Ammar, F. Chinesta, E. Cueto, M. Doblaré, Proper generalized decomposition of time-multiscale models, Int. J. Numer. Methods Eng. 90 (5) (2012) 569–596.
[51] F. Jedrzejewski, Introduction to Numerical Methods, Springer-Verlag, Paris, 2005 (in French).
[52] F. Chinesta, A. Ammar, A. Leygue, R. Keunings, An overview of the proper generalized decomposition with applications in computational rheology, J. Non-Newtonian Fluid Mech. 166 (June (11)) (2011) 578–592.
[53] D. González, F. Masson, F. Poulhaon, A. Leygue, E. Cueto, F. Chinesta, Proper generalized decomposition based dynamic data driven inverse identification, Math. Comput. Simul. 82 (May (9)) (2012) 1677–1695.
[54] F. Chinesta, A. Ammar, E. Cueto, Proper generalized decomposition of multiscale models, Int. J. Numer. Methods Eng. 83 (August (8–9)) (2010) 1114–1132.
[55] P.O. Fanger, Fundamental of thermal comfort, in: W.H. Blos, F. Pfisterer (Eds.), Advances in Solar Energy Technology, Pergamon, 1988, pp. 3056–3061.
[56] H. Viitanen, Moisture and biodeterioration risk of building materials and structure, J. Build. Phys. 33 (3) (2010) 201–224.
[57] J. Berger, Contribution á la modélisation hygrothermique des bâtiments: application des méthodes de réduction de modèles (Ph.D. thesis), Universite de Savoie Montblanc, December 2014 (in French).
[58] J.L.M. Hensen, Modelling Coupled Heat and Air Flow: Ping-pong vs Onions, IEA Air Infiltration and Ventilation Centre, Coventry, UK, September 1995, pp. 253–262.
[59] H.J. Moon, Assessing Mold Risks in Buildings Under Uncertainty (Ph.D. thesis), Georgia Institute of Technology, 2005.